HHS Public Access

Author manuscript

*Neuroendocrinology*. Author manuscript; available in PMC 2017 April 05.

Published in final edited form as:

*Neuroendocrinology*. 2017 ; 104(3): 239–256. doi:10.1159/000446073.

# Redistribution of NMDA Receptors in Estrogen-Receptor-β-Containing Paraventricular Hypothalamic Neurons following Slow-Pressor Angiotensin II Hypertension in Female Mice with Accelerated Ovarian Failure

**Jose Marques-Lopes**[a], **Ephrath Tesfaye**[a], **Sigal Israilov**[a], **Tracey A. Van Kempen**[a,b], **Gang Wang**[a], **Michael J. Glass**[a,b], **Virginia M. Pickel**[a,b], **Costantino Iadecola**[a,b], **Elizabeth M. Waters**[c], and **Teresa A. Milner**[a,b,c]

[a]Feil Family Brain and Mind Research Institute, The Rockefeller University, New York, N.Y., USA

[b]Weill Cornell Graduate School of Medical Sciences, Weill Cornell Medicine, The Rockefeller University, New York, N.Y., USA

[c]Harold and Margaret Milliken Hatch Laboratory of Neuroendocrinology, The Rockefeller University, New York, N.Y., USA

## Abstract

Hypertension in male and aging female rodents is associated with glutamate-dependent plasticity in the hypothalamus, but existing models have failed to capture distinct transitional menopausal phases that could have a significant impact on the synaptic plasticity and emergent hypertension. In rodents, accelerated ovarian failure (AOF) induced by systemic injection of 4-vinylcyclohexane diepoxide mimics the estrogen fluctuations seen in human menopause including the perimenopause transition (peri-AOF) and postmenopause (post-AOF). Thus, we used the mouse AOF model to determine the impact of slow-pressor angiotensin II (AngII) administration on blood pressure and on the subcellular distribution of obligatory N-methyl-D-aspartate (NMDA) receptor GluN1 subunits in the paraventricular hypothalamic nucleus (PVN), a key estrogen-responsive cardiovascular regulatory area. Estrogen-sensitive neuronal profiles were identified in mice expressing enhanced green fluorescent protein under the promoter for estrogen receptor (ER) β, a major ER in the PVN. Slow-pressor AngII increased arterial blood pressure in mice at peri- and post-AOF time points. In control oil-injected (nonhypertensive) mice, AngII decreased the total number of GluN1 in ERβ-containing PVN dendrites. In contrast, AngII resulted in a reapportionment of GluN1 from the cytoplasm to the plasma membrane of ERβ-containing PVN dendrites in peri-AOF mice. Moreover, in post-AOF mice, AngII increased total GluN1, dendritic size and radical production in ERβ-containing neurons. These results indicate that unique patterns of hypothalamic glutamate receptor plasticity and dendritic structure accompany the elevated blood pressure in peri- and post-AOF time points. Our findings suggest the possibility that distinct

Teresa A. Milner, Feil Family Brain and Mind Research Institute, Weill Cornell Medicine, 407 East 61st Street, RM 307, New York, NY 10065 (USA), tmilner@med.cornell.edu.

**Disclosure Statement**

The authors declare no competing financial interests.

neurobiological processes are associated with the increased blood pressure during perimenopausal and postmenopausal periods.

**Keywords**

Hypertension; Paraventricular nucleus; Estrogens; Perimenopause; Neural plasticity

## Introduction

The prevalence of hypertension is greater in men than in young women, but this relationship is reversed as women progress into menopause [1, 2]. The transitional phase preceding and extending through menopause (i.e. perimenopause; ages 45–54 years) is thought to be a critical period for the brain plasticity that fosters the development of hypertension in older females [3]. The perimenopausal phase is accompanied by irregular menstrual cycles and erratically fluctuating estrogen levels [4, 5] and by increased sympathetic tone [6] . A sex-dependent susceptibility to hypertension is recapitulated in rodents following systemic administration of low doses of angiotensin II (AngII). In young male mice, but not cycling young female mice, systemic low-dose AngII infusion results in a slowly developing (i.e. slow-pressor) increase in sympathetic tone and blood pressure [7–12]. However, slow-pressor AngII infusion induces hypertension in ovariectomized mice that model surgical menopause [12, 13] and in aged rodents [8, 10, 14] that model the acyclicity [15] seen in postmenopause. Unfortunately, neither of these approaches has been able to elucidate potential mechanisms related to ovarian hormone irregularity and decline that contribute to perimenopausal hypertension. We addressed this gap in knowledge by using a mouse model of accelerated ovarian failure (AOF) that uniquely recapitulates hormonal changes seen in human menopause including the menopause transition while controlling for the effects of aging [16, 17].

The emergence of hypertension in males, as well as in aging models of menopause, has been associated with glutamate-dependent plasticity in the hypothalamus [8, 9, 18–20]. The hypothalamic paraventricular nucleus (PVN) receives a prominent glutamate input from the AngII-sensitive subfornical organ, and this circuit is crucial for the sympathoexcitation underlying slow-pressor AngII-induced hypertension [21–23]. In males, upregulation of postsynaptic N-methyl-D-aspartate (NMDA) receptor function in PVN neurons that project to the spinal cord may play a pivotal role in the enhanced excitatory drive seen in hypertension models [24–26]. Activated NMDA receptors can stimulate nicotinamide adenine dinucleotide phosphate (NADPH) oxidase activity, generating reactive oxygen species (ROS), leading to the activation of voltage-gated L-type $Ca^{2+}$ currents [7, 27, 28] . AngII-induced hypertension enhances ROS production, which is linked to augmentation of the obligatory NMDA GluN1 receptor subunit on the plasmalemmal surface of PVN neurons [8, 9, 18, 29–31]. Importantly, spatiotemporal deletion of the NMDA GluN1 subunit in the PVN dampens local ROS production and attenuates AngII-induced hypertension in males [18]. Although it is presumed that NMDA receptor activation increases ROS in the PVN in hypertensive females, the ability of estrogen to influence NMDA receptor activation in other brain areas [32] does not preclude different outcomes.

In young females, normal estrogen production and estrous cycling may play a key role in attenuating AngII-induced hypertension [12, 13] . Posttranscriptional gene silencing studies have revealed that these protective effects of estrogen on hypertension and ROS production critically involve estrogen receptor (ER) β, but not ERα, in the PVN [33] . In the PVN, estradiol activation of ERβ tempers the glutamate-induced increase in blood pressure [34]. Moreover, our recent electron microscopy studies [8, 9, 20] revealed that alterations in the subcellular distributions of GluN1 in ERβ-containing PVN neurons reflect the hypertensive responses of male and female mice following slow-pressor AngII. In particular, the density of GluN1 is elevated in hypertensive male and aged female mice but decreased in nonhypertensive young females. However, estrogen levels of aged mice are not completely depleted [35], and it is difficult to disentangle the effects of aging from hormonal effects. Thus, findings in aged mice may not accurately reflect subcellular changes in GluN1 trafficking following AngII-induced hypertension at time points that model the peri-menopause transition or postmenopause in humans.

In the present study, we used the recently established mouse model of AOF first to determine whether mice at the ‘perimenopausal’ time point are susceptible to slow-pressor AngII-induced hypertension. Second, we sought to determine whether the hypertensive responses of AOF mice at ‘peri-’ and ‘post-menopausal’ time points are reflected by changes in the density and/or trafficking of the GluN1 subunit in ERβ-expressing dendrites. Third, we examined whether slow-pressor AngII in AOF mice at a ‘postmenopausal’ time point leads to changes in NMDA-evoked ROS production in ERβ-expressing neurons. These results were first presented as an abstract at the Society for Neuroscience Annual Meeting [36].

## Methods

### Animals

Experimental procedures were approved by the Institutional Animal Care and Use Committee of Weill Cornell Medicine and were in accordance with the 2011 Eighth Edition of the National Institute of Health Guide for the Care and Use of Laboratory Animals. Studies were conducted in bacterial artificial chromosome ERβ-enhanced green fluorescent protein (ERβ-EGFP) mice on a C57BL/6 background [37] . Briefly, ERβ-EGFP mice were originally developed by the GENSAT project (www.gensat.org) at the Rockefeller University [38] . Hemizygote bacterial artificial chromosome-based ERβ transgenic mice were originally bred on an FVB/N background and were backcrossed with wild-type C57BL/6 mice for 6 generations. Three to four mice were housed per cage with 12-hour light/12-hour dark cycles with ad libitum access to food and water. The GFP genotype was verified using hot-start PCR reagent kits (Qiagen, Valencia, Calif., USA) and a Flash gel system (Lonza, Rockland, Maine, USA).

### AOF Induction and Estrous Cycle Determination

Previous studies demonstrate that the mouse model of AOF uniquely recapitulates hormonal changes seen in human menopause [16, 17, 39, 40]. Injections of low doses of 4-vinylcyclohexene diepoxide (VCD) selectively eliminate primary follicles in the ovary and, following ovarian failure, result in undetectable levels of estradiol [39, 40]. Several studies

have confirmed that VCD administration does not negatively affect peripheral tissues, including organ weights and liver and kidney function [41–44]. Recently, we have shown that VCD does not have any direct effects on the brain areas inside (e.g. PVN, hippocampus) and outside (e.g. sub-fornical organ, area postrema) the blood-brain barrier [17].

A schematic of the timeline of the experiments is shown in online supplementary figure 1 (for all online suppl. material, see www.karger.com/doi/10.1159/000446073). To induce AOF, gonadally intact 50- to 55-postnatal-day-old female mice (n = 78) were injected with VCD (130 mg/kg i.p.) in vehicle (sesame oil) for 5 sequential days per week for 3 weeks as described previously [17] . Control mice were injected with oil (vehicle) only. Littermates were randomly selected for oil or VCD injection. The estrous cycle stage was assessed using vaginal smear cytology [45]. Estrous cycle assessment was performed 8–10 days prior to osmotic minipump insertion.

Time points following VCD injections in mice corresponding to pre-, peri-, and postmenopausal stages in humans have been previously determined [17, 39, 40]. At the pre-AOF time point (23 days following initiation of VCD injections; 2.7 months old), mice have regular 4- to 5-day-long estrous cycles, which consist of 3 primary phases: proestrus (high estrogen levels; 0.5–1 day), estrus (declining estrogen levels; 2–2.5 days) and diestrus (low estrogen and progesterone levels; 2–2.5 days) [17]. At the peri-AOF time point (58 days following initiation of VCD injections and corresponding to ‘perimenopause’; 4 months old), mice have irregular and extended estrous cycles and increased plasma follicle-stimulating hormone similar to the human perimenopause [4, 39, 40]. At the peri-AOF time point, only 50% of the mice have a normal cyclicity [17]. The gradual hormonal changes seen in the AOF mice across the menopause transition are similar to those observed in humans and contrast with those seen following ovariectomy in which estrogen levels are undetectable [16]. At the post-AOF time point (129 days following initiation of VCD injections and corresponding to ‘postmenopause’; 6.5 months old), mice show an acyclic, anestrous status, in which persistent estrus is observed and ovulation has ceased [17]. At the post-AOF time point, the VCD-injected mice have undetectable serum levels of estrogen, decreased levels of progesterone as well as elevated serum levels of luteinizing hormone, follicle-stimulating hormone and androstenedione (reviewed in Van Kempen et al. [16]).

### Slow-Pressor AngII Administration

To minimize stress, the mice were handled by the same experimenter (J.M.-L.) and at the same time of day throughout the study. Under isoflurane anesthesia, osmotic minipumps (Alzet, Durect Corporation, Cupertino, Calif., USA) containing vehicle (saline + 0.1% bovine serum albumin) or AngII (600 ng $\cdot$ kg$^{-1}$ $\cdot$ min$^{-1}$) were implanted subcutaneously in pre-AOF (oil/saline: n = 7; VCD/saline: n = 5; oil/AngII: n = 6; VCD/AngII: n = 7), peri-AOF (oil/saline: n = 6; VCD/saline: n = 4; oil/AngII: n = 4; VCD/AngII: n = 5) and post-AOF mice (oil/saline: n = 6; VCD/saline: n = 9; oil/AngII: n = 9; VCD/AngII: n = 7). Systolic blood pressure (SBP) was measured before (baseline), and 2, 5, 9, and 13 days after minipump implantation in awake mice by tail cuff plethysmography (Model MC4000; Hatteras Instruments, Cary, N.C., USA), as described previously [46]. Tail cuff plethysmography is a reliable measurement for comparing SBP between groups [8, 9, 29,

31, 46, 47]. The limitations of tail cuff plethysmography to measure blood pressure have been discussed previously [8]. Tail cuff plethysmography is particularly suited to assess the brain perfusion required for electron microscopy-level tissue fixation [48], because it is noninvasive and does not sacrifice the carotid artery, unlike telemetric blood pressure recording in mice [49]. To control for handling effects, mice were euthanized 1 day after the final SBP measurements (i.e. 14 days after pump implantation) [8, 9, 29, 31].

## Immunocytochemical Procedures

**Antibody Characterization—**For labeling of EGFP, a chicken polyclonal anti-GFP antibody (GFP-1020; RRID: AB_10000240; Aves Lab Inc., San Diego, Calif., USA) was used. The GFP antibody was generated against recombinant GFP and recognizes the gene product of EGFP-expressing transgenic mice [50]. The specificity of this antibody has been demonstrated by immunohistochemistry and Western blot using transgenic mice that express GFP, resulting in one major band at 27 kD (see data sheet for EGFP-1020 at www.aveslab.com). Moreover, absence of labeling has been shown in brain sections from mice not expressing EGFP [48, 51]. The labeling of EGFP in ERβ-EGFP-expressing mice closely corresponds to that reported for ERβ protein and mRNA [37] . The specificity of the anti-ERβ antisera (Z8P; RRID: AB_87720; Zymed Laboratories, San Francisco, Calif., USA) used to validate the fidelity of the ERβ-EGFP-expressing mice in the study of Milner et al. [37] has been shown by (1) dual labeling with mRNA using in situ hybridization, (2) preadsorption control, and (3) absence of labeling in brain sections from ERβ knockout mice [52, 53]. This is important as the majority of commercially available antibodies to ERβ lack specificity [54].

To identify GluN1 (the NMDA receptor 1 protein encoded by the Grin1 gene), a monoclonal mouse anti-GluN1 antibody (clone 54.1; RRID: AB_86917; BD Biosciences, San Diego, Calif., USA) was used. Reduced labeling for this antiserum has been shown following rAAV-Cre administration into the brain of floxed GluN1 mice [55, 56]. Specificity of the GluN1 antibody was characterized via immunoprecipitation and immunohistochemistry [57–59]. Western blot analysis of rat synaptic membranes and monkey hippocampal homogenates probed with the GluN1 antibody resulted in one major band at 116 kD. HEK 293 cells transfected with cDNA encoding GluN1 displayed similar results, whereas non-transfected cells resulted in no bands [58].

**Tissue Preparation—**The brains of mice from the peri-AOF (~4.5 months old) and post-AOF (~6.5 months old) time points were prepared for electron-microscopic studies [48]. For this, mice were deeply anesthetized with sodium pentobarbital (150 mg/kg, i.p.) and fixed by aortic arch perfusion sequentially with 3–5 ml saline (0.9%) containing 2% heparin followed by 30 ml of 3.75% acrolein and 2% paraformaldehyde in 0.1 M phosphate buffer (PB) [48]. After the perfusion, brains were removed and postfixed for 30 min in 2% acrolein and 2% paraformaldehyde in PB at room temperature. Brains were then cut into 5-mm coronal blocks using a brain mold (Activational Systems Inc., Warren, Mich., USA) and sectioned (40 μm thick) on a VT1000X vibratome (Leica Microsystems, Buffalo Grove, Ill., USA). Brain sections were stored at –20°C in cryoprotectant (30% sucrose, 30% ethylene glycol in PB) until immunocytochemical processing.

To ensure identical labeling conditions between experimental groups for quantitative immunocytochemistry [60] , 2 sections per animal (3 animals per group) encompassing the region of the PVN (0.70–0.94 mm caudal to bregma; fig. 2a [61]) were marked with identifying punches, pooled into single containers and then processed together through all immunocytochemical procedures.

### Dual-Label Electron-Microscopic Immunocytochemistry

Tissue sections were processed using a pre-embedding dual immunolabeling protocol, as described previously [48]. The tissue was treated with 1% sodium borohydride in PB for 30 min to neutralize reactive aldehydes and rinsed thoroughly in PB. The free-floating sections were then immersed in 0.5% bovine serum albumin in 0.1 M Tris-buffered saline for 30 min. The tissue was then incubated at room temperature in a solution of anti-GluN1 (1: 50) antiserum in 0.1 M Tris-buffered saline with 0.1% bovine serum albumin for 48 h. Anti-GFP (1: 2,500) antiserum was added to the primary antibody diluent at 24 h, and the tissue was moved to 4°C.

For immunoperoxidase detection of GFP, sections were placed for 30 min in goat anti-chicken IgG (1: 400; Jackson Immunoresearch Inc., West Grove, Pa., USA), followed by a 30-min incubation in avidin-biotin complex (Vector Laboratories, Burlingame, Calif., USA). After rinsing in Tris-buffered saline, the bound peroxidase was visualized by reaction of the sections for 6 min in 3,3′-diaminobenzidine (Sigma-Aldrich Chemical Co., Milwaukee, Mich., USA) and hydrogen peroxide.

For immunogold detection of GluN1, the diaminobenzidine-reacted sections were rinsed and incubated overnight in a 1: 50 dilution of donkey anti-mouse IgG with bound 1-nm colloidal gold [Electron Microscopy Sciences (EMS), Fort Washington, Pa., USA]. The tissue was placed in a solution of 2% glutaraldehyde in 0.01 M phosphate-buffered saline (pH 7.4) and then rinsed in phosphate-buffered saline followed by 0.2 M sodium citrate buffer (pH 7.4). Bound gold particles were enhanced using a Silver IntenSEM kit (RPN491; GE Healthcare, Waukeska, Wisc., USA) for 7 min.

Tissue sections were postfixed in 2% osmium tetroxide for 1 h, dehydrated through a series of graded ethanols and propylene oxide, and flat-embedded in Embed-812 (EMS) between two sheets of Aclar plastic. Ultrathin sections (70 nm thickness) from the PVN (see fig. 2a for schematic) were cut with a diamond knife (EMS) using a Leica EM UC6 ultratome. The sections were collected on 400-mesh thin-bar copper grids (EMS) and counter-stained with uranyl acetate and lead citrate.

### Ultrastructural Data Analyses

A person blind to the experimental conditions performed the data collection and analysis. Sections were examined using a Tecnai transmission electron microscope. Images were collected at a magnification of ×18,500. Profiles containing GluN1 with GFP immunoreactivity were classified as neuronal (soma, dendrites, axons, terminals) or glial based on criteria described by Peters et al. [62] . Dendritic profiles contained regular microtubular arrays and were usually postsynaptic to axon terminal profiles.

An equal amount of tissue from each treatment group (9,596 μm $^2$ /group) was sampled for electron-microscopic analysis as described previously [48] . In each block, 50 dual-labeled dendritic profiles were randomly selected from the tissue-plastic interface and photographed. Usually, 1 thin section per block was sufficient to obtain the required number of dendritic profiles. Occasionally, 2 sections per block were analyzed. In this case, the profiles were taken from nonoverlapping regions of the block. Immunoperoxidase labeling for GFP was distinguished as a precipitous electron-dense reaction product. Silver-intensified immunogold (SIG) labeling for GluN1 appeared as black electron-dense particles. To avoid false-negative labeling of smaller structures, they were considered as dual-labeled if they contained electron-dense reaction product and at least 1 gold particle. Criteria for field selection included good morphological preservation, the presence of immunolabeling in the field, and proximity to the plastic-tissue interface (i.e. the surface of the tissue) to avoid problems due to differences in antibody penetration [48].

The subcellular distribution and density of GluN1-SIG particles in ERβ-EGFP-labeled dendrites was determined as previously described [29] . For this, Microcomputer Imaging Device software (Imaging Research Inc., Ont., Canada) was used to determine cross-sectional diameter, perimeter (i.e. plasmalemma), surface area, form factor, and major and minor axis lengths of each immunolabeled dendrite. Dendrites with an oblong or irregular shape (form factor value <0.5) were excluded from the data set. The parameters used for statistical comparisons were as follows: (1) the number of plasmalemmal GluN1-SIG particles on the dendrite/unit plasma membrane perimeter (μm), (2) the number of near-plasmalemmal GluN1-SIG particles that were located within 70 nm of, but not touching, the plasma membrane/unit plasma membrane perimeter (μm), (3) the number of cytoplasmic GluN1-SIG particles/dendritic cross-sectional area (μm $^2$), and (4) the total number of GluN1-SIG particles (sum of plasmalemmal, near-plasmalemmal and cytoplasmic) in a dendritic profile/unit cross-sectional area (μm $^2$). The partitioning ratio is the proportion of GluN1-SIG particles in a particular subcellular compartment (e.g. plasma membrane or cytoplasm) divided by the total number of GluN1-SIG particles. Dendrites were further divided into small (≤ 1.0 μm) and large (>1.0 μm) based on average diameter, which correspond to distal and proximal to the cell body [62]. Dendritic area and average diameter were also compared across all groups.

## ROS Detection

ROS production was determined using dihydroethidium (DHE; Life Technologies). Superoxide oxidizes the cell-permanent DHE to 2-hydroxyethidium and other oxidation products [63, 64], which interact with DNA and are detectable using an ethidium bromide (ETH) filter (Chroma Technology, Rockingham, Vt., USA) on a Nikon Eclipse C-CU microscope. ROS production was measured in dissociated PVN cells from oil- or VCD-injected female mice at the post-AOF time point after 14 days of vehicle or AngII infusion (n = 13–19 cells/group, from 4–5 mice each), as described previously [29] . Dissociation and identification of ERβ-EGFP PVN cells was performed as described previously [9]. Methods for ROS detection in dissociated cells using DHE have been previously described [7]. Briefly, isolated PVN cells were incubated in DHE (2 μM) containing lactate-artificial cerebrospinal fluid for 30 min. Time-resolved fluorescence using IPLab software

(Scanalytics, Fairfax, Va., USA) was measured at 1-min intervals with an exposure time of 150 ms for 40 min using a Nikon Diaphot 300 inverted microscope equipped with a CCD digital camera (Princeton Instruments, Trenton, N.J., USA). Bath application of 100 μM NMDA was performed after a stable baseline measurement for 10 min. NMDA is known to induce NOX2-dependent free radical production in the brain [7] . The increase in ROS signal induced by NMDA was expressed as the ratio of Ft/Fo, where Ft is fluorescence after application of NMDA, and Fo is the baseline fluorescence in the same cell [7, 9, 31]. For analysis of NMDA-induced ROS signals, the baseline background intensity was subtracted from the detected ETH signals in targeted cells.

### Statistical Analysis

Two-way ANOVA was used to compare SBP values, SIG particle density and ROS production. Significant interactions were further analyzed with Tukey's HSD post hoc test. Data were expressed as means ± SEM. Values were considered statistically significant when $p < 0.05$.

### Figure Preparation

Images were adjusted for brightness, contrast and sharpness in Adobe Photoshop 9.0. These changes did not alter the original content of the raw image. Graphs were generated in Prism 5 (GraphPad Software, La Jolla, Calif., USA). Final figures were made in PowerPoint 2010.

## Results

### Estrous Cycle Assessment of AOF Mice

For mice used in the electron-microscopic studies, the estrous cycle was assessed using vaginal smear cytology 8–10 days prior to implanting osmotic minipumps (online suppl. table 1). Consistent with previous studies [17], oil-injected mice from all time points and VCD-injected mice from the pre-AOF time point exhibited 4- to 5-day-long estrous cycles. In contrast, the estrous cycles from the peri-AOF VCD-injected mice were irregular and often lacked the proestrous (high-estrogen) phase of the cycle. Moreover, all but 1 of the post-AOF VCD-injected mice were acyclic. The 1 post-AOF VCD mouse that was not acyclic had an irregular estrous cycle.

The final estrous phase was collected on the day of euthanasia (i.e. 14 days after implantation of the osmotic minipumps). Final estrous phases for peri- and post-AOF mice used in the electron microscopy studies are provided in online supplementary table 2. Oil-injected mice from the peri- and post-AOF time points exhibited estrous phases from all points of the cycle. In contrast, no VCD-injected mice from the peri- or post-AOF time point had a final proestrous phase. Peri-AOF VCD mice had equal proportions of estrous and metestrous/diestrous phases in the saline- and AngII-infused groups. All but 1 of the post-AOF VCD mice were in metestrus/diestrus on the day of euthanasia; the remaining post-AOF VCD mouse was in estrus.

The estrous cycle was also assessed using vaginal smear cytology prior to minipump implantation and at the termination of the study for most of the mice used in the other

portions of the study (online suppl. table 2). In these mice, the pattern of estrous cycle stages for the various time points (pre-, peri- and post-AOF) and treatments (oil vs. VCD) was similar to those seen in the mice used for the electron microscopy studies.

### Slow-Pressor AngII Increases SBP in Peri- and Post-AOF Female Mice

There were no significant differences in blood pressure prior to osmotic minipump implantation (i.e. baseline) or on days 2, 5, and 9 after implantation in mice injected with vehicle (oil) or VCD (online suppl. table 3). On day 13 after minipump implantation, there were significant main effects of AOF time point [$F(3, 69) = 3.98$, $p < 0.05$] and saline/AngII administration [$F(1, 69) = 15.63$, $p < 0.001$], as well as a significant time point × An-gII administration interaction [$F(3, 36) = 4.18$, $p = 0.01$] on blood pressure. Consistently with previous studies [7–9, 12, 65], slow-pressor AngII administration failed to increase blood pressure in oil-injected mice or in pre-AOF VCD mice (fig. 1). However, post hoc analysis revealed that AngII induced a significant increase in blood pressure both at the peri- ($p < 0.001$) and post-AOF ($p < 0.001$) time points in the VCD mice (fig. 1). The elevation in blood pressure at both of these menopausal stages was comparable to that observed in male mice [8, 18, 29, 66].

### Distribution of ERβ-EGFP-Labeled Cells in the PVN

In all groups, the topographic distribution of ERβ-EGFP-labeled neurons in the PVN as well as the subcellular localization of GluN1-SIG particles in ERβ-EGFP dendrites was similar. Consistently with previous light-microscopic observations [8, 37], a dense cluster of ERβ-EGFP-containing cells was observed in the PVN (fig. 2a, b). At higher magnification, thick, dendrite-like processes of ERβ-EGFP neurons were visualized (fig. 2b, inset).

By electron microscopy, GluN1-SIG particles were easily identifiable in the cytoplasm, near the plasmalemma, and on the plasma membrane of ERβ-EGFP-containing dendrites (fig. 2c). Within the cytoplasm, GluN1-SIG particles were often adjacent to endomembranes (fig. 2c). GluN1-SIG particles were also observed in ERβ-EGFP-labeled terminals and somata, and in non-ERβ-containing dendrites, terminals, and glia (not shown). Numerous terminals, some of which formed asymmetric synapses, contacted ERβ-EGFP-containing dendrites. Samples for electron-microscopic analysis were selected from PVN regions containing ERβ-EGFP-labeled neurons as identified in plastic embedding material by light microscopy.

### Electron-Microscopic Analysis of the Distribution of GluN1 in PVN ERβ-EGFP in Dendrites

Since slow-pressor AngII increased blood pressure in the peri- and post-AOF VCD-injected mice, the electron-microscopic analysis was limited to these two time points. We assessed the distribution of GluN1-SIG particles in ERβ-EGFP-containing dendrites of PVN neurons in oil- and VCD-injected mice following either saline or slow-pressor AngII infusion. The initial statistical analysis showed no significant differences in either the densities or partitioning ratios of GluN1-SIG particles in oil-injected (control) mice from peri- and post-AOF time points following either saline or AngII infusions. Thus, control groups from the two time points were pooled into one saline and one AngII control group.

Both time point (control, peri- and post-AOF) and treatment (oil, AngII) influenced the subcellular distribution of GluN1-SIG particles in ERβ-EGFP-containing dendrites. Two-way ANOVA of cytoplasmic GluN1-SIG density in ERβ-EGFP-containing dendrites showed a main effect of AOF time point [$F(2, 853) = 9.61$, $p < 0.001$] and saline/AngII administration [$F(1, 853) = 8.51$, $p < 0.01$]. Similarly, analysis of the total GluN1-SIG density in ERβ-EGFP-containing dendrites revealed a main effect of AOF time point [$F(2, 1,077) = 9.89$, $p < 0.001$] and saline/AngII administration [$F(1, 1,077) = 8.25$, $p < 0.01$], and a significant AOF time point × AngII administration interaction [$F(2, 1,077) = 10.60$, $p < 0.001$]. The post hoc results for saline-administered (i.e. baseline) and AngII-administered mice will be presented separately below. Representative micrographs from each group (control, peri- and post-AOF) and treatment are shown in figure 3.

**In Saline-Infused Mice, the Baseline Densities of GluN1 Distributions Varied with AOF Time Point—**Baseline levels of the distribution of GluN1-SIG particles in ERβ-EGFP-containing dendrites at different AOF time points were compared in saline-infused mice from different AOF time points. The density of GluN1-SIG particles in the cytoplasm of ERβ-EGFP dendrites in post-AOF VCD-injected mice was significantly less than in oil-injected (control) mice ($p < 0.05$) and peri-AOF VCD-injected mice ($p < 0.05$; fig. 3a, c, e, 4a). Similarly, the total density of GluN1 in ERβ-EGFP dendrites in post-AOF VCD-injected saline-infused mice was significantly less than in oil-injected (control) mice ($p < 0.001$) and peri-AOF VCD-injected mice ($p < 0.01$) infused with saline (fig. 4b).

**Following Slow-Pressor AngII, GluN1 Density in ERβ-EGFP Dendrites Varies with AOF Time Point—**Following slow-pressor AngII, redistribution of GluN1-SIG particles within ERβ-EGFP-containing dendrites varied depending on group (oil vs. VCD), time point after VCD injections (peri- or post-AOF) and hypertensive response. In the peri-AOF VCD-injected mice, the cytoplasmic density of GluN1-SIG particles in ERβ-EGFP dendrites was significantly decreased ($p < 0.01$) following slow-pressor AngII (fig. 3c, d, 4a). However, no differences in cytoplasmic labeling were observed in oil-injected controls and in post-AOF VCD (hypertensive) females (fig. 4a) following slow-pressor AngII. Slow-pressor AngII significantly reduced the total density of GluN1-SIG particles in ERβ-EGFP dendrites in both oil-injected controls and peri-AOF VCD-injected mice ($p < 0.001$; fig. 3a–d, 4b). Conversely, slow-pressor AngII significantly increased ($p < .05$) the total density of GluN1-SIG particles in ERβ-EGFP dendrites from post-AOF VCD-injected mice (fig. 3e, f, 4b).

The functional specialization of distal and proximal dendritic compartments contributes to both signal conduction and synaptic plasticity [67, 68]. Thus, we further analyzed GluN1-SIG density in small and large ERβ-EGFP dendrites, which correspond to distal and proximal dendrites, respectively [62]. Two-way ANOVA showed a main effect of saline/AngII administration on the density of GluN1-SIG particles in the cytoplasm [$F(1, 685) = 14.60$, $p < 0.001$] in small (≤ 0.1 μm in diameter) ERβ-EGFP dendrites. Following slow-pressor AngII, peri- and post-AOF VCD mice had reduced densities of cytoplasmic ($p < 0.01$; fig. 4c) GluN1-SIG particles in small ERβ-EGFP dendritic profiles compared to saline-injected VCD mice.

Two-way ANOVA showed a main effect of AOF time point [$F(2, 1,077) = 9.89$, $p < 0.001$] and AngII administration [$F(1, 1,077) = 8.25$, $p < 0.01$], and a significant interaction between AOF time point and AngII administration [$F(2, 1,077) = 10.60$, $p < 0.001$] in the total GluN1 density in small ERβ-EGFP dendrites. The density of total GluN1-SIG particles in small ERβ-EGFP dendritic profiles was significantly reduced ($p < 0.01$) in peri-AOF VCD mice and in oil-injected (control) mice infused with AngII compared to peri-AOF mice infused with saline (fig. 4d).

In all groups, large dual-labeled dendrites (>1 μm in diameter) comprised 17.5 ± 1.8% ($n = 8$) of the total dendritic profiles. Two-way ANOVA showed a main effect of AngII [$F(2, 204) = 5.049$, $p < 0.05$) and a significant interaction between AOF time point and AngII administration [$F(2, 204) = 4.285$, $p < 0.05$) in the cytoplasmic density of GluN1 in ERβ-EGFP dendrites. However, post hoc analysis showed no significant differences between groups ( fig. 4e). Two-way ANOVA also showed a main effect of AngII [$F(2, 219) = 4.177$, $p < 0.05$] and a significant interaction between AOF time point and AngII administration [$F(2, 219) = 5.081$, $p < 0.05$] in the total density of GluN1 in ERβ-EGFP dendrites. The density of total GluN1 in ERβ-EGFP dendrites was significantly less ($p < 0.05$) in the oil-injected (control) mice only (fig. 4f).

**Following Slow-Pressor AngII, the GluN1 Plasma Membrane Partitioning Ratio in ERβ-EGFP Dendrites Varies with Induction of Hypertension and AOF Time Point—**Two-way ANOVA showed a main effect of saline/An-gII administration [$F(1, 910) = 6.60$, $p < 0.05$] and a significant interaction of AOF time point × AngII administration [$F(2, 1,077) = 5.83$, $p < 0.01$] in the partitioning ratio in the near-plasmalemmal + plasmalemmal compartments in ERβ-EGFP dendrites. The proportion of plasma membrane-associated (i.e. plasma membrane + near-plasma membrane) GluN1-SIG particles on ERβ-EGFP dendrites was significantly higher ($p < 0.01$) in peri-AOF VCD-injected mice following AngII compared to those that were infused with saline. No significant changes in the plasma membrane partitioning ratio of GluN1 were seen in either the oil-injected (control) or the post-AOF VCD mice following AngII infusion (fig. 5a).

The cytoplasmic partitioning ratio of GluN1-SIG particles in ERβ-EGFP dendrites was altered in different groups than that seen with the plasma membrane partitioning ratio. Two-way ANOVA of the cytoplasmic GluN1-SIG partitioning ratio in ERβ-EGFP dendrites revealed a main effect of AOF time point [$F(2, 933) = 6.60$, $p < 0.01$] and a significant AOF time point × AngII administration interaction [$F(2, 933) = 9.66$, $p < 0.001$]. Slow-pressor AngII did not alter the cytoplasmic partitioning ratio of GluN1 in ERβ-EGFP dendrites from peri-AOF VCD-injected mice (fig. 5b). however, the proportion of cytoplasmic GluN1 in ERβ-EGFP dendrites was significantly increased ($p < 0.05$) in oil-injected (control) mice infused with AngII compared to those infused with saline. Moreover, the proportion of cytoplasmic GluN1 in ERβ-EGFP dendrites was significantly decreased ($p < 0.05$) in the post-AOF VCD-injected mice infused with AngII compared to those infused with saline (fig. 5b). Also, the partitioning ratio of cytoplasmic to total GluN1-SIG particles in ERβ-EGFP-containing dendrites was significantly less ($p < 0.001$) in post-AOF VCD mice infused with AngII compared to oil-injected mice infused with AngII (fig. 5b).

### AngII Affects the Morphology of GluN1-ERβ-EGFP Dendrites in Post-AOF Mice

—The morphological measurements (i.e. area and diameter) were compared in dendrites dually labeled for GluN1 and ERβ-EGFP in the different groups (control, peri- and post-AOF) and treatments (saline, AngII). Two-way ANOVA showed main effects of AOF time point [$F(2, 1,133) = 4.05$, $p < 0.05$] and saline/AngII administration [$F(1, 1,133) = 9.71$, $p < 0.01$], as well as a significant interaction of AOF time point × AngII administration [$F(2, 1,133) = 7.65$, $p < 0.01$] with respect to the area of dual-labeled dendritic profiles. Post hoc analysis showed that the area ($p < 0.01$; fig. 6a) of GluN1/ERβ-EGFP-containing dendritic profiles was significantly greater in post-AOF VCD mice that were infused with AngII compared to those infused with saline. Similarly, two-way ANOVA showed a main effect of saline/AngII administration [$F(1, 1,133) = 6.93$, $p < 0.01$] and a significant AOF time point × AngII interaction [$F(2, 1,133) = 3.93$, $p < 0.05$] with respect to the diameter of dually labeled dendrites. Post hoc analysis showed that average diameters ($p < 0.01$; fig. 6b) of GluN1/ERβ-EGFP-containing dendritic profiles were significantly greater in post-AOF VCD mice that were infused with AngII compared to those infused with saline. No differences in the area or diameter of dual-labeled dendrites were observed in peri-AOF mice or in oil-injected control mice following AngII (fig. 6a, b).

## Following Slow-Pressor AngII, ROS Production Is Increased in ERβ-EGFP PVN Cells in Post-AOF Females

NADPH oxidase-generated ROS are thought to play a critical role in AngII-induced hypertension and are also associated with increased NMDA receptor activity in male mice [9, 18, 29, 69]. To determine whether ROS are elevated following slow-pressor AngII hypertension, females from the pre- and post-AOF time points were selected for analysis. For this experiment, ROS production was analyzed in dissociated ERβ-EGFP PVN cells from VCD-injected mice and oil-injected mice that were infused with either saline or AngII. ROS levels were measured in ERβ-EGFP cells at baseline (i.e. in the presence of vehicle in the bath) and after NMDA application (fig. 7a).

In the pre-AOF mice, there were no significant group (oil vs. VCD) or treatment (saline vs. AngII) differences in ROS production in ERβ-EGFP cells at baseline or following NMDA (100 μm) application (not shown). In contrast, two-way ANOVA showed a main effect of saline/AngII [$F(3, 121) = 14.23$, $p < 0.001$] and NMDA administration [$F(3, 121) = 8.45$, $p = 0.0034$] on ROS production in ERβ-EGFP cells from the post-AOF time point. In oil-injected (control) mice, ROS production in ERβ-EGFP PVN cells was not significantly different at baseline or following NMDA (100 μm) application following either saline or AngII infusion (fig. 7b). However, slow-pressor AngII significantly ($p < 0.05$) increased baseline levels of ROS in ERβ-EGFP PVN cells from post-AOF VCD-injected mice compared to their saline-infused controls (fig. 7b). Moreover, application of NMDA to ERβ-EGFP cells from AngII-infused VCD mice significantly elevated ROS production ($p < 0.001$) compared to saline-infused mice (fig. 7b).

## Discussion

Our study provides the first evidence that susceptibility to slow-pressor AngII hypertension and NMDA receptor plasticity emerge at a point in ovarian decline that mimics perimenopause in a mouse model of AOF. Quantitative electron microscopy immunogold-silver labeling revealed that, in the absence of AngII, saline-infused control (oil-injected) and peri-AOF VCD females have greater densities of GluN1 in PVN ERβ-containing dendrites than post-AOF VCD females. Following slow-pressor AngII infusion, the induction of hypertension is accompanied by AOF time point-dependent changes in GluN1 subcellular distribution in ERβ-EGFP PVN dendrites, which are not seen in control nonhypertensive mice that show a decrease in total GluN1 expression in these dendrites. In hypertensive peri-AOF mice, GluN1-SIG particles were more prevalent on and near the plasma membrane and less abundant in the cytoplasm of ERβ-containing dendrites. In hypertensive post-AOF mice, total GluN1, dendritic size as well as radical production increased in ERβ-containing neurons. The results summarized in figure 8 identify 'perimenopause' as a critical period for the induction of changes in NMDA receptor distributions in estrogen-sensitive neurocardiovascular regulatory systems involved in AngII hypertension.

### Susceptibility to Slow-Pressor AngII Hypertension Emerges at the Peri-AOF Time Point

The present studies using the AOF model together with studies in ovariectomized and aging female mice have reinforced the importance of the regular cycling of ovarian hormones, particularly estrogens, in protecting females from hypertension susceptibility. Like young adult females with normal estrous cycles [7–9, 12, 20, 65], slow-pressor AngII infusion did not elevate blood pressure in control (oil-injected) or pre-AOF VCD-injected females. In addition, similarly to ovariectomized mice in which all ovarian hormones, including estrogens, are removed [11, 65], we demonstrate that slow-pressor AngII induces hypertension in post-AOF mice which have undetectable serum levels of estrogen [for a review, see 16]. Our studies also demonstrate in an animal model that susceptibility to slow-pressor AngII-induced hypertension emerges at a time point that mimics perimenopausal hormonal levels. It is important to note that at the peri-AOF time point, the mice have irregular estrous cycles with fewer proestrous (elevated plasma estrogen) stages [for a review, see 16 ]. Thus, these results suggest that deregulation of estrogen cyclicity rather than the absence of estrogen is the major contributor to the emergence of hypertension susceptibility. Previous studies [8, 10] showing that slow-pressor AngII induces hypertension in aged females, which are acyclic and usually in prolonged estrus, support this assertion.

### ERβ PVN Neurons Are Important for Central Cardiovascular Regulatory Networks

Our finding that AngII-induced hypertension in peri- and post-AOF mice is accompanied by changes in GluN1 distribution and ROS production in ERβ-containing PVN neurons adds to the growing body of literature supporting a prominent role for ERβ in cardiovascular regulatory networks. In particular, previous studies have shown that knockdown of ERβ, but not ERα, mediates protective effects of estrogen against aldosterone/salt-induced hypertension in rats [33]. Moreover, our previous studies showed that slow-pressor AngII

does not alter GluN1 distribution in non-ERβ-containing PVN neurons in either males or females [9, 20].

In rodents, the PVN contains numerous neurons with both nuclear and extranuclear ERβ [37, 52, 70, 71]. The ERβ reporter mice used in the present study identify neurons with ERβ in either location [37]. Although the rodent PVN harbors ERα-containing neurons, these are proportionally much fewer than those containing ERβ [72, 73]. However, studies describing the proportions of ERβ- and ERα-containing neurons in human postmortem tissue not only depend on age, gender and reproductive menopausal status, but also on whether nuclear or cytoplasmic ERβ is measured. Compared to nuclear ERα, lower levels of nuclear ERβ immunoreactivity and mRNA are found in the human PVN [74–76] . In contrast, the proportion of cells with cytoplasmic ERβ immunoreactivity is greater than cells with cytoplasmic ERα immunoreactivity in women but not men [75].

In rodents, ERβ is present in PVN neurons that project to the intermediolateral spinal cord and rostral ventrolateral medulla [8, 77, 78]. Thus, ERβ-containing PVN neurons are positioned to regulate sympathoexcitation both directly and indirectly [79]. The phenotype of ERβ-containing neurons in the PVN is less clear as it appears to be species dependent. In mice, ERβ-containing neurons lack arginine vasopressin [37] and angiotensin 1a receptors [9]. The finding that ERβ-containing PVN neurons in mice lack arginine vasopressin is consistent with some studies in the rat [80, 81] but not with others [71, 82, 83] . However, the topographic distribution of ERβ-containing neurons in mice resembles that of parvicellular neurons [84] and is consistent with findings in rats showing that many ERβ-containing PVN neurons colocalize corticotropin-releasing factor [77, 81] . Like ERβ-containing neurons, previous studies in rats show that corticotropin-releasing factor neurons project to the spinal cord [77]. Our results, together with those in the literature, suggest that ERβ activation of spinal output neurons in the mouse PVN regulate sympathetic activity mainly through the increased release of transmitters co-stored with corticotropin-releasing factor and not vasopressin.

### Baseline Levels of GluN1 in ERβ PVN Dendrites Vary with AOF Time Point

Our electron-microscopic analysis showed baseline differences in the subcellular distribution of GluN1 in ERβ-EGFP PVN dendrites from saline-infused mice, which varied depending on AOF time point. Oil-injected (control) females had higher cytoplasmic and total GluN1-SIG densities in ERβ-containing dendrites compared to post-AOF females. Although these results are consistent with previous studies comparing young and aged ‘postmenopausal’ female mice [8], they are not identical. In particular, total and near-plasmalemmal GluN1-SIG densities in ERβ-containing dendrites are reduced in aged compared to young females. Several factors could contribute to these differences. The oil-injected mice in this study were slightly older than the young mice (4–6 vs. 2–3 months) in our previous study. Unlike the young female mice, the oil-injected mice were handled and injected for 3 weeks prior to implanting osmotic mini-pumps. Additionally, as mentioned above, the estrogen levels in the aged mice are reduced but not depleted as in the AOF postmenopausal mice.

Interestingly, GluN1-SIG densities in ERβ-containing dendrites in peri-AOF females shared characteristics with both the control (oil-injected) and post-AOF females: cytoplasmic

GluN1-SIG densities were elevated as in young females [8] but total GluN1-SIG densities were decreased as in post-AOF females. Cytoplasmic receptors may be stored, in transit to/from the cell body or other cellular compartments as well as in the process of recycling [85, 86]. Thus, this finding indicates that more NMDA receptors in ERβ-containing dendrites from peri-AOF females may be accessible for mobilization to the plasma membrane in response to neuronal activation.

## AngII Hypertension in Peri-AOF Mice Is Accompanied by an Increase in Plasmalemmal Associated GluN1 in ERβ PVN Dendrites

Slow-pressor AngII administration was associated with reduced total GluN1-SIG particles in ERβ-EGFP dendrites in control (oil-injected) nonhypertensive females. This observation was consistent with our previous study [8] showing that slow-pressor AngII resulted in decreased cytoplasmic and total GluN1 in ERβ-EGFP dendrites in young (2-month-old) nonhypertensive females. However, in the peri-AOF females, in which slow-pressor AngII resulted in hypertension, a different distributional profile of GluN1 in ERβ-containing dendrites emerged. In contrast to oil-injected female mice, the proportion of near-plasmalemma plus plasmalemma GluN1-SIG particles relative to total GluN1-SIG particles *increased* in peri-AOF mice after AngII. As the presence of plasmalemmal receptors corresponds to sites of ligand binding [87, 88], our findings suggest that more GluN1 is available for glutamate binding on the ERβ-containing dendrites in the peri-AOF mice. Greater activation of ERβ-containing neurons, many of which project to the spinal cord [37, 77], would be consistent with increased sympathoexcitation seen in hypertension at the peri-AOF time point.

Slow-pressor AngII infusion resulted in a decreased cytoplasmic density of GluN1-SIG particles in ERβ-containing dendrites in hypertensive peri-AOF females. This decrease in GluN1-SIG density was more robust in small dendrites, which are more numerous than large dendrites and generally receive a higher number of excitatory-type inputs [67, 68]. The decrease in cytoplasmic GluN1 may reflect an activity-dependent decrease in GluN1 synthesis or association with the endomembranes located in closer proximity to the plasmalemma [89]. In contrast to peri-AOF females, slow-pressor AngII infusion resulted in a greater proportion of cytoplasmic GluN1 in ERβ-containing dendrites relative to total GluN1 in the nonhypertensive oil-injected mice. This would be consistent with GluN1 accumulation in association with cytosolic compartments distant from the plasma membrane and/or in storage [85, 86]. Moreover, as baseline levels of cytoplasmic and total GluN1 labeling in peri-AOF and control mice are similar, the dysregulated estrous cycle and/or erratically fluctuating estrogen levels seen in peri-AOF mice may disrupt the protection from susceptibility to slow-pressor AngII hypertension.

Several lines of evidence suggest that the repositioning of GluN1 to the plasmalemma of ERβ-containing PVN dendrites predominantly involves ERβ or related signaling pathways. Activation of surface-affiliated ERβ can transduce intracellular signaling cascades linked to a number of kinases (e.g. PI3K/Akt/mTOR, PLC, ERK1/2, PKC, and PKA) and phosphatases that can regulate plasma membrane NMDA receptor transport to or away from the plasma membrane [90–92] . ERβ activation can modulate NMDA receptor signaling in

various brain regions [93–95] . In the hippocampus, knockout of ERβ abolishes estradiol-induced elevations in phosphorylated Akt, a major regulator of synaptic plasticity [96]. Also, in young ovariectomized rats, estradiol regulates the synaptic distributions of NMDA receptors, ERβ and phosphorylated Akt (reviewed in McEwen et al. [97]). In contrast to ERβ, PVN neurons express few nuclear and extranuclear ERα that are also important regulators of NMDA receptor synaptic plasticity (reviewed in McEwen et al. [98] ; Milner, unpubl. observations). Thus, without ERα to balance out ERβ, even small disruptions in ERβ signaling would be expected to alter NMDA receptor-dependent excitability in PVN neurons.

## AngII Hypertension in Post-AOF Mice Is Largely Independent of GluN1 Surface Trafficking in ERβ Dendrites Which Are Larger and Contain More Total GluN1 than Controls

Although slow-pressor AngII induced hypertension in post-AOF females, GluN1-SIG particles in ERβ-containing dendrites did not reapportion to the plasma membrane as they did in peri-AOF females. Instead, slow-pressor AngII-induced hypertension in the post-AOF females occurred together with a small increase in total GluN1 density and a decreased cytoplasmic-to-total ratio of GluN1 in the ERβ-containing dendrites. This difference in the redistribution pattern of GluN1 may be because at the post-AOF time point the baseline levels of plasmalemmal GluN1 are already equivalent to the AngII-induced levels of GluN1 seen in the peri-AOF mice. Moreover, as estrogen levels had been depleted for over 1 month in the post-AOF mice, estrogen-mediated NMDA receptor excitability could have been compromised. This assertion is supported by finding that the ability of estradiol to increase synaptic ERβ as well as related signaling molecules is much more limited in the aged rat hippocampus [99, 100]. Second, long-term depletion of ovarian hormones after ovariectomy reduces intrinsic membrane excitability of CA1 pyramidal cells [101]. The limited redistribution of GluN1 in dendrites from post-AOF mice following AngII infusion may also indicate the involvement of other mechanisms in the induction of AngII hypertension at this AOF time point.

Concomitantly with these changes in GluN1 densities, the size of the ERβ-containing dendrites increased in the post-AOF mice showing slow-pressor AngII hypertension. This increase in dendritic size could reflect disruption in membrane endocytosis or blockage of receptor recycling leading to an accumulation in the plasma membrane [102]. However, we cannot exclude the alternative possibility that AngII infusion sufficient to produce slow-pressor hypertension in post-AOF mice may preferentially increase GluN1 retention in large, presumably more proximal ERβ dendrites in the PVN. Regardless of the underlying causes, the increased dendritic size and differential responsivity of GluN1 in ERβ PVN dendrites to AngII infusion in post-AOF mice provide mutually supportive evidence that favors the involvement of separate mechanisms in AngII hypertension in peri- and post-menopausal periods.

## AngII Hypertension in Post-AOF Mice Is Associated with NMDA-Evoked ROS Production in ERβ PVN Neurons

Our findings that ROS production is not elevated in ERβ-containing cells from post-AOF VCD mice receiving saline or in pre-AOF mice demonstrate that neither the injection

procedure nor the AOF time point is sufficient to elevate ROS production in these PVN neurons. However, AngII-induced hypertension in post-AOF female mice is accompanied by an elevation in baseline and NMDA-stimulated ROS production in ERβ-containing PVN neurons compared to saline-infused mice. Thus, like males [9, 29, 31, 69], NADPH oxidase-mediated ROS production in the PVN is critically involved in AngII-induced hypertension and is associated with increased NMDA activity in post-AOF females. The finding that estradiol administration to ovariectomized females improves redox balance by reducing NADPH oxidase activity and inhibiting ROS production [66, 103] suggests that estrogen is importantly involved in the sensitivity of post-AOF females to AngII.

Our recent studies [29, 104] suggest that the sensitivity of PVN neurons to AngII-induced NADPH oxidase ROS production may be phenotype specific depending on sex. The Nox2 isoform of NADPH oxidase requires mobilization of cytoplasmic p47 $^{phox}$ to dock with the membrane-bound proteins for superoxide production [105]. In the PVN of hypertensive males, baseline ROS production is increased in nonvasopressin neurons accompanied by an increase in near-plasmalemmal p47 $^{phox}$ in nonvasopressin dendrites and decreased plasmalemmal p47 $^{phox}$ in vasopressin dendrites [29]. In contrast, AngII-induced hypertension in post-AOF females increases near-plasmalemmal p47 $^{phox}$ in arginine vasopres-sin dendrites [104]. While nonvasopressin PVN neurons comprise mixed phenotypes including ERβ [8, 37, 84], these data suggest that the differential response of various neuronal populations in males and females may contribute to hypertensive changes.

## Functional Considerations

In addition to affecting glutamate-dependent plasticity in the PVN, changes in hormone levels at the peri- and post-AOF time points could contribute to the pathology of hypertension through alternative mechanisms. These include regulation of superoxide-generating NADPH oxidase, intracellular calcium and angiotensin receptor signaling [for reviews, see 106 and also 104]. Additionally, in male rats experimentally induced hypertension can be modulated by nuclear factor-κB in the PVN [107] as well as activity of the $K^+/Cl^-$ cotransporter, a molecule required for inhibitory $GABA_A$ receptor signaling [108]. Thus, future studies using the AOF model will explore these alternative mechanisms.

Our studies provide new evidence that hypertension susceptibility emerges at the ‘perimenopause’ using the AOF mouse model that recapitulates hormonal changes seen in human menopause [16, 17]. Slow-pressor AngII-induced hypertension in AOF females is accompanied by enhanced superoxide production and NMDA-mediated signaling in PVN ERβ-containing dendrites similar to that observed previously in males [29, 31]. Moreover, AngII-induced hypertension in peri-AOF mice results in a compartmental shift in the subcellular distribution of GluN1 toward plasma membranes of PVN ERβ-containing dendrites, where GluN1 NMDA receptors would be available for glutamate binding and thus enhancing sympathoexcitation. Importantly, within the PVN NMDA receptor, redistribution in ERβ-containing dendrites is greatly diminished in hypertensive post-AOF mice. These findings are consistent with a growing body of clinical evidence [109, 110] that the perimenopausal period is a ‘window of opportunity’ for gonadal steroid replacement therapy to modulate hypertension susceptibility.

## Supplementary Material

Refer to Web version on PubMed Central for supplementary material.

## Acknowledgments

This work was supported by: NIH grants HL098351, DA08259 and AG016765 (to T.A.M.), HL096571 (to C.I., V.M.P., M.J.G., T.A.M.), AG059850 (to E.M.W.), and T32 DA007274 (to T.A.K.). We thank Ms. Mariana Dodos for assistance in making the figures.

## References

1. Martins D, Nelson K, Pan D, Tareen N, Norris K. The effect of gender on age-related blood pressure changes and the prevalence of isolated systolic hypertension among older adults: data from NHANES III. J Gend Specif Med. 2001; 4:10–13. 20. [PubMed: 11605350]
2. Maranon R, Reckelhoff JF. Sex and gender differences in control of blood pressure. Clin Sci (Lond). 2013; 125:311–318. [PubMed: 23746374]
3. Towfighi A, Saver JL, Engelhardt R, Ovbiagele B. A midlife stroke surge among women in the United States. Neurology. 2007; 69:1898–1904. [PubMed: 17581944]
4. Harsh V, Schmidt PJ, Rubinow DR. The menopause transition: the next neuroendocrine frontier. Expert Rev Neurother. 2007; 7:S7–S10. [PubMed: 18039070]
5. Nejat EJ, Chervenak JL. The continuum of ovarian aging and clinicopathologies associated with the menopausal transition. Maturitas. 2010; 66:187–190. [PubMed: 20462711]
6. Rosano GM, Vitale C, Marazzi G, Volterrani M. Menopause and cardiovascular disease: the evidence. Climacteric. 2007; 10(suppl 1):19–24. [PubMed: 17364594]
7. Girouard H, Wang G, Gallo EF, Anrather J, Zhou P, Pickel VM, Iadecola C. NMDA receptor activation increases free radical production through nitric oxide and NOX2. J Neurosci. 2009; 29:2545–2552. [PubMed: 19244529]
8. Marques-Lopes J, Van Kempen T, Waters EM, Pickel VM, Iadecola C, Milner TA. Slow-pressor angiotensin II hypertension and concomitant dendritic NMDA receptor trafficking in estrogen receptor beta-containing neurons of the mouse hypothalamic paraventricular nucleus are sex and age dependent. J Comp Neurol. 2014; 522:3075–3090. [PubMed: 24639345]
9. Marques-Lopes J, Lynch MK, Van Kempen TA, Waters EM, Wang G, Iadecola C, Pickel VM, Milner TA. Female protection from slow-pressor effects of angiotensin II involves prevention of ROS production independent of NMDA receptor trafficking in hypothalamic neurons expressing angiotensin 1A receptors. Synapse. 2015; 69:148–165. [PubMed: 25559190]
10. Tiwari S, Li L, Riazi S, Halagappa VK, Ecelbarger CM. Sex and age result in differential regulation of the renal thiazide-sensitive NaCl cotransporter and the epithelial sodium channel in angiotensin II-infused mice. Am J Nephrol. 2009; 30:554–562. [PubMed: 19844087]
11. Xue B, Pamidimukkala J, Hay M. Sex differences in the development of angiotensin II-induced hypertension in conscious mice. Am J Physiol Heart Circ Physiol. 2005; 288:H2177–H2184. [PubMed: 15626687]
12. Xue B, Johnson AK, Hay M. Sex differences in angiotensin II- and aldosterone-induced hypertension: the central protective effects of estrogen. Am J Physiol Regul Integr Comp Physiol. 2013; 305:R459–R463. [PubMed: 23883676]
13. Hay M, Xue B, Johnson AK. Yes! Sex matters: sex, the brain and blood pressure. Curr Hypertens Rep. 2014; 16:458. [PubMed: 24929952]
14. Fortepiani LA, Zhang H, Racusen L, Roberts LJ 2nd, Reckelhoff JF. Characterization of an animal model of postmenopausal hypertension in spontaneously hypertensive rats. Hypertension. 2003; 41:640–645. [PubMed: 12623972]
15. Nelson JF, Karelus K, Bergman MD, Felicio LS. Neuroendocrine involvement in aging: evidence from studies of reproductive aging and caloric restriction. Neurobiol Aging. 1995; 16:837–843. [PubMed: 8532119]

16. Van Kempen TA, Milner TA, Waters EM. Accelerated ovarian failure: a novel, chemically induced animal model of menopause. Brain Res. 2011; 1379:176–187. [PubMed: 21211517]
17. Van Kempen TA, Gorecka J, Gonzalez AD, Soeda F, Milner TA, Waters EM. Characterization of neural estrogen signaling and neurotrophic changes in the accelerated ovarian failure mouse model of menopause. Endocrinology. 2014; 155:3610–3623. [PubMed: 24926825]
18. Glass MJ, Wang G, Coleman CG, Chan J, Ogorodnik E, Van Kempen TA, Milner TA, Butler SD, Young CN, Davisson RL, Iadecola C, Pickel VM. NMDA receptor plasticity in the hypothalamic paraventricular nucleus contributes to the elevated blood pressure produced by angiotensin II. J Neurosci. 2015; 35:9558–9567. [PubMed: 26134639]
19. Li DP, Pan HL. Glutamatergic inputs in the hypothalamic paraventricular nucleus maintain sympathetic vasomotor tone in hypertension. Hypertension. 2007; 49:916–925. [PubMed: 17309953]
20. Van Kempen TA, Dodos M, Woods C, Marques-Lopes J, Justice NJ, Iadecola C, Pickel VM, Glass MJ, Milner TA. Sex differences in NMDA GluN1 plasticity in rostral ventrolateral medulla neurons containing corticotropin-releasing factor type 1 receptor following slow-pressor angiotensin II hypertension. Neuroscience. 2015; 307:83–97. [PubMed: 26306872]
21. Carmichael CY, Wainford RD. Hypothalamic signaling mechanisms in hypertension. Curr Hypertens Rep. 2015; 17:39. [PubMed: 25860531]
22. De Wardener HE. The hypothalamus and hypertension. Physiol Rev. 2001; 81:1599–1658. [PubMed: 11581498]
23. Osborn JW, Fink GD, Sved AF, Toney GM, Raizada MK. Circulating angiotensin II and dietary salt: converging signals for neurogenic hypertension. Curr Hypertens Rep. 2007; 9:228–235. [PubMed: 17519130]
24. Li DP, Pan HL. Increased group I metabo-tropic glutamate receptor activity in paraventricular nucleus supports elevated sympathetic vasomotor tone in hypertension. Am J Physiol Regul Integr Comp Physiol. 2010; 299:R552–R561. [PubMed: 20519363]
25. Li DP, Yang Q, Pan HM, Pan HL. Pre- and postsynaptic plasticity underlying augmented glutamatergic inputs to hypothalamic pre-sympathetic neurons in spontaneously hypertensive rats. J Physiol. 2008; 586:1637–1647. [PubMed: 18238817]
26. Li DP, Zhu LH, Pachuau J, Lee HA, Pan HL. mGluR5 upregulation increases excitability of hypothalamic presympathetic neurons through NMDA receptor trafficking in spontaneously hypertensive rats. J Neurosci. 2014; 34:4309–4317. [PubMed: 24647951]
27. Wang G, Anrather J, Glass MJ, Tarsitano MJ, Zhou P, Frys KA, Pickel VM, Iadecola C. Nox2, $Ca^{2+}$, and protein kinase C play a role in angiotensin II-induced free radical production in nucleus tractus solitarius. Hypertension. 2006; 48:482–489. [PubMed: 16894058]
28. Wang G, Milner TA, Speth RC, Gore AC, Wu D, Iadecola C, Pierce JP. Sex differences in angiotensin signaling in bulbospinal neurons in the rat rostral ventrolateral medulla. Am J Physiol Regul Integr Comp Physiol. 2008; 295:R1149–R1157. [PubMed: 18685065]
29. Coleman CG, Wang G, Faraco G, Marques Lopes J, Waters EM, Milner TA, Iadecola C, Pickel VM. Membrane trafficking of NADPH oxidase p47(phox) in paraventricular hypothalamic neurons parallels local free radical production in angiotensin II slow-pressor hypertension. J Neurosci. 2013; 33:4308–4316. [PubMed: 23467347]
30. Jancovski N, Bassi JK, Carter DA, Choong YT, Connelly A, Nguyen TP, Chen D, Lukoshkova EV, Menuet C, Head GA, Allen AM. Stimulation of angiotensin type 1A receptors on catecholaminergic cells contributes to angiotensin-dependent hypertension. Hypertension. 2013; 62:866–871. [PubMed: 24001896]
31. Wang G, Coleman CG, Chan J, Faraco G, Marques-Lopes J, Milner TA, Guruju MR, Anrather J, Davisson RL, Iadecola C, Pickel VM. Angiotensin II slow-pressor hypertension enhances NMDA currents and NOX2-dependent superoxide production in hypothalamic paraventricular neurons. Am J Physiol Regul Integr Comp Physiol. 2013; 304:R1096–R1106. [PubMed: 23576605]
32. Woolley CS, Weiland NG, McEwen BS, Schwartzkroin PA. Estradiol increases the sensitivity of hippocampal CA1 pyramidal cells to NMDA receptor-mediated synaptic input: correlation with dendritic spine density. J Neurosci. 1997; 17:1848–1859. [PubMed: 9030643]

33. Xue B, Zhang Z, Beltz TG, Johnson RF, Guo F, Hay M, Johnson AK. Estrogen receptor-beta in the paraventricular nucleus and rostroventrolateral medulla plays an essential protective role in aldosterone/salt-induced hypertension in female rats. Hypertension. 2013; 61:1255–1262. [PubMed: 23608653]
34. Gingerich S, Krukoff TL. Estrogen in the paraventricular nucleus attenuates L-glutamate-induced increases in mean arterial pressure through estrogen receptor beta and NO. Hypertension. 2006; 48:1130–1136. [PubMed: 17075034]
35. Maffiucci, J., Gore, A. Age-related changes in hormones and their receptors in animal models of female reproductive senescence. In: Conn, PM., editor. Handbook of Models for Human Aging. San Diego: Academic Press; 2006. p. 533-552.
36. Marques-Lopes, J., Tesfaye, E., Israilov, S., Van, Kempen TA., Wang, G., Iadecola, C., Waters, EM., Milner, TA. Susceptibility to hypertension emerges at peri-menopause and is accompanied by elevations in plasma membrane post-synaptic NMDA receptors and reactive oxygen species production in estrogen receptor β-containing neurons in the mouse paraventricular hypothalamic nucleus. Soc Neurosci Annu Meet; Chicago. 2015.
37. Milner TA, Thompson LI, Wang G, Kievits JA, Martin E, Zhou P, McEwen BS, Pfaff DW, Waters EM. Distribution of estrogen receptor beta containing cells in the brains of bacterial artificial chromosome transgenic mice. Brain Res. 2010; 1351:74–96. [PubMed: 20599828]
38. Gong S, Zheng C, Doughty ML, Losos K, Didkovsky N, Schambra UB, Nowak NJ, Joyner A, Leblanc G, Hatten ME, Heintz N. A gene expression atlas of the central nervous system based on bacterial artificial chromosomes. Nature. 2003; 425:917–925. [PubMed: 14586460]
39. Lohff JC, Christian PJ, Marion SL, Arrandale A, Hoyer PB. Characterization of cyclicity and hormonal profile with impending ovarian failure in a novel chemical-induced mouse model of perimenopause. Comp Med. 2005; 55:523–527. [PubMed: 16422148]
40. Mayer LP, Devine PJ, Dyer CA, Hoyer PB. The follicle-deplete mouse ovary produces androgen. Biol Reprod. 2004; 71:130–138. [PubMed: 14998904]
41. Haas JR, Christian PJ, Hoyer PB. Effects of impending ovarian failure induced by 4-vinylcyclohexene diepoxide on fertility in C57BL/6 female mice. Comp Med. 2007; 57:443–449. [PubMed: 17974126]
42. Sahambi SK, Visser JA, Themmen AP, Mayer LP, Devine PJ. Correlation of serum anti-mullerian hormone with accelerated follicle loss following 4-vinylcyclohexene diepoxide-induced follicle loss in mice. Reprod Toxicol. 2008; 26:116–122. [PubMed: 18706995]
43. Wright LE, Christian PJ, Rivera Z, Van Alstine WG, Funk JL, Bouxsein ML, Hoyer PB. Comparison of skeletal effects of ovariectomy versus chemically induced ovarian failure in mice. J Bone Miner Res. 2008; 23:1296–1303. [PubMed: 18348702]
44. Mayer LP, Dyer CA, Eastgard RL, Hoyer PB, Banka CL. Atherosclerotic lesion development in a novel ovary-intact mouse model of perimenopause. Arterioscler Thromb Vasc Biol. 2005; 25:1910–1916. [PubMed: 15994440]
45. Turner, C., Bagnara, J. General Endocrinology. Philadelphia: Saunders; 1971.
46. Coleman CG, Wang G, Park L, Anrather J, Delagrammatikas GJ, Chan J, Zhou J, Iadecola C, Pickel VM. Chronic intermittent hypoxia induces NMDA receptor-dependent plasticity and suppresses nitric oxide signaling in the mouse hypothalamic paraventricular nucleus. J Neurosci. 2010; 30:12103–12112. [PubMed: 20826673]
47. Capone C, Faraco G, Anrather J, Zhou P, Iadecola C. Cyclooxygenase 1-derived prostaglandin E2 and EP1 receptors are required for the cerebrovascular dysfunction induced by angiotensin II. Hypertension. 2010; 55:911–917. [PubMed: 20194308]
48. Milner TA, Waters EM, Robinson DC, Pierce JP. Degenerating processes identified by electron microscopic immunocytochemical methods. Methods Mol Biol. 2011; 793:23–59. [PubMed: 21913092]
49. Butz GM, Davisson RL. Long-term telemetric measurement of cardiovascular parameters in awake mice: a physiological genomics tool. Physiol Genomics. 2001; 5:89–97. [PubMed: 11242593]
50. Encinas JM, Vaahtokari A, Enikolopov G. Fluoxetine targets early progenitor cells in the adult brain. Proc Natl Acad Sci USA. 2006; 103:8233–8238. [PubMed: 16702546]

51. Volkmann K, Chen YY, Harris MP, Wullimann MF, Koster RW. The zebrafish cerebellar upper rhombic lip generates tegmental hindbrain nuclei by long-distance migration in an evolutionary conserved manner. J Comp Neurol. 2010; 518:2794–2817. [PubMed: 20506476]
52. Shughrue PJ, Merchenthaler I. Distribution of estrogen receptor beta immunoreactivity in the rat central nervous system. J Comp Neurol. 2001; 436:64–81. [PubMed: 11413547]
53. Creutz LM, Kritzer MF. Estrogen receptor-beta immunoreactivity in the midbrain of adult rats: regional, subregional, and cellular localization in the A10, A9, and A8 dopamine cell groups. J Comp Neurol. 2002; 446:288–300. [PubMed: 11932944]
54. Snyder MA, Smejkalova T, Forlano PM, Woolley CS. Multiple ERbeta antisera label in ERbeta knockout and null mouse tissues. J Neurosci Methods. 2010; 188:226–234. [PubMed: 20170675]
55. Beckerman MA, Glass MJ. The NMDA-NR1 receptor subunit and the mu-opioid receptor are expressed in somatodendritic compartments of central nucleus of the amygdala neurons projecting to the bed nucleus of the stria terminalis. Exp Neurol. 2012; 234:112–126. [PubMed: 22227057]
56. Glass MJ, Hegarty DM, Oselkin M, Quimson L, South SM, Xu Q, Pickel VM, Inturrisi CE. Conditional deletion of the NMDA-NR1 receptor subunit gene in the central nucleus of the amygdala inhibits naloxone-induced conditioned place aversion in morphine-dependent mice. Exp Neurol. 2008; 213:57–70. [PubMed: 18614169]
57. Brose N, Huntley GW, Stern-Bach Y, Sharma G, Morrison JH, Heinemann SF. Differential assembly of coexpressed glutamate receptor subunits in neurons of rat cerebral cortex. J Biol Chem. 1994; 269:16780–16784. [PubMed: 8207001]
58. Siegel SJ, Brose N, Janssen WG, Gasic GP, Jahn R, Heinemann SF, Morrison JH. Regional, cellular, and ultrastructural distribution of N-methyl-D-aspartate receptor subunit 1 in monkey hippocampus. Proc Natl Acad Sci USA. 1994; 91:564–568. [PubMed: 8290563]
59. Siegel SJ, Janssen WG, Tullai JW, Rogers SW, Moran T, Heinemann SF, Morrison JH. Distribution of the excitatory amino acid receptor subunits GluR2(4) in monkey hippocampus and colocalization with subunits GluR5–7 and NMDAR1. J Neurosci. 1995; 15:2707–2719. [PubMed: 7722624]
60. Pierce JP, Kurucz OS, Milner TA. Morphometry of a peptidergic transmitter system: dynorphin B-like immunoreactivity in the rat hippocampal mossy fiber pathway before and after seizures. Hippocampus. 1999; 9:255–276. [PubMed: 10401641]
61. Hof, P., Young, W., Bloom, F., Belinchenko, P., Ceilo, M. Comparative Cytoarchitectonic Atlas of the C57BL/6 and 129/SV Mouse Brains. 1. Amsterdam: Elsevier; 2000.
62. Peters, A., Palay, S., Webster, H. The Fine Structure of the Nervous System. New York: Oxford University Press; 1991.
63. Zhao H, Joseph J, Fales HM, Sokoloski EA, Levine RL, Vasquez-Vivar J, Kalyanaraman B. Detection and characterization of the product of hydroethidine and intracellular superoxide by HPLC and limitations of fluorescence. Proc Natl Acad Sci USA. 2005; 102:5727–5732. [PubMed: 15824309]
64. Zhao H, Kalivendi S, Zhang H, Joseph J, Nithipatikom K, Vasquez-Vivar J, Kalyanaraman B. Superoxide reacts with hydroethidine but forms a fluorescent product that is distinctly different from ethidium: potential implications in intracellular fluorescence detection of superoxide. Free Radic Biol Med. 2003; 34:1359–1368. [PubMed: 12757846]
65. Xue B, Singh M, Guo F, Hay M, Johnson AK. Protective actions of estrogen on angiotensin II-induced hypertension: role of central nitric oxide. Am J Physiol Heart Circ Physiol. 2009; 297:H1638–H1646. [PubMed: 19734362]
66. Xue B, Zhao Y, Johnson AK, Hay M. Central estrogen inhibition of angiotensin II-induced hypertension in male mice and the role of reactive oxygen species. Am J Physiol Heart Circ Physiol. 2008; 295:H1025–H1032. [PubMed: 18599599]
67. Froemke RC, Poo MM, Dan Y. Spike-timing-dependent synaptic plasticity depends on dendritic location. Nature. 2005; 434:221–225. [PubMed: 15759002]
68. Lovett-Barron M, Kaifosh P, Kheirbek MA, Danielson N, Zaremba JD, Reardon TR, Turi GF, Hen R, Zemelman BV, Losonczy A. Dendritic inhibition in the hippocampus supports fear learning. Science. 2014; 343:857–863. [PubMed: 24558155]

69. Erdos B, Broxson CS, King MA, Scarpace PJ, Tumer N. Acute pressor effect of central angiotensin II is mediated by NAD(P)H-oxidase-dependent production of superoxide in the hypothalamic cardiovascular regulatory nuclei. J Hypertens. 2006; 24:109–116. [PubMed: 16331108]
70. Mitra SW, Hoskin E, Yudkovitz J, Pear L, Wilkinson HA, Hayashi S, Pfaff DW, Ogawa S, Rohrer SP, Schaeffer JM, McEwen BS, Alves SE. Immunolocalization of estrogen receptor beta in the mouse brain: comparison with estrogen receptor alpha. Endocrinology. 2003; 144:2055–2067. [PubMed: 12697714]
71. Hrabovszky E, Kallo I, Steinhauser A, Merchenthaler I, Coen CW, Petersen SL, Liposits Z. Estrogen receptor-beta in oxytocin and vasopressin neurons of the rat and human hypothalamus: immunocytochemical and in situ hybridization studies. J Comp Neurol. 2004; 473:315–333. [PubMed: 15116394]
72. Merchenthaler I, Lane MV, Numan S, Dellovade TL. Distribution of estrogen receptor alpha and beta in the mouse central nervous system: in vivo autoradiographic and immunocytochemical analyses. J Comp Neurol. 2004; 473:270–291. [PubMed: 15101093]
73. Milner TA, Drake CT, Lessard A, Waters EM, Torres-Reveron A, Graustein B, Mitterling K, Frys K, Iadecola C. Angiotensin II-induced hypertension differentially affects estrogen and progestin receptors in central autonomic regulatory areas of female rats. Exp Neurol. 2008; 212:393–406. [PubMed: 18533148]
74. Kruijver FP, Balesar R, Espila AM, Unmehopa UA, Swaab DF. Estrogen receptor-alpha distribution in the human hypothalamus in relation to sex and endocrine status. J Comp Neurol. 2002; 454:115–139. [PubMed: 12412138]
75. Kruijver FP, Balesar R, Espila AM, Unmehopa UA, Swaab DF. Estrogen-receptor-beta distribution in the human hypothalamus: similarities and differences with ER alpha distribution. J Comp Neurol. 2003; 466:251–277. [PubMed: 14528452]
76. Osterlund MK, Gustafsson JA, Keller E, Hurd YL. Estrogen receptor beta (ERbeta) messenger ribonucleic acid (mRNA) expression within the human forebrain: distinct distribution pattern to ERalpha mRNA. J Clin Endocrinol Metab. 2000; 85:3840–3846. [PubMed: 11061547]
77. Bingham B, Williamson M, Viau V. Androgen and estrogen receptor-beta distribution within spinal-projecting and neurosecretory neurons in the paraventricular nucleus of the male rat. J Comp Neurol. 2006; 499:911–923. [PubMed: 17072840]
78. Stern JE, Zhang W. Preautonomic neurons in the paraventricular nucleus of the hypothalamus contain estrogen receptor beta. Brain Res. 2003; 975:99–109. [PubMed: 12763597]
79. Benarroch EE. Paraventricular nucleus, stress response, and cardiovascular disease. Clin Autonom Res. 2005; 15:254–263.
80. Alves SE, Lopez V, McEwen BS, Weiland NG. Differential colocalization of estrogen receptor beta (ERbeta) with oxytocin and vasopressin in the paraventricular and supraoptic nuclei of the female rat brain: an immunocytochemical study. Proc Natl Acad Sci USA. 1998; 95:3281–3286. [PubMed: 9501254]
81. Laflamme N, Nappi RE, Drolet G, Labrie C, Rivest S. Expression and neuropeptidergic characterization of estrogen receptors (ER-alpha and ERbeta) throughout the rat brain: anatomical evidence of distinct roles of each subtype. J Neurobiol. 1998; 36:357–378. [PubMed: 9733072]
82. Hrabovszky E, Kallo I, Hajszan T, Shughrue PJ, Merchenthaler I, Liposits Z. Expression of estrogen receptor-beta messenger ribonucleic acid in oxytocin and vasopressin neurons of the rat supraoptic and paraventricular nuclei. Endocrinology. 1998; 139:2600–2604.
83. Somponpun SJ, Sladek CD. Osmotic regulation of estrogen receptor-beta in rat vasopressin and oxytocin neurons. J Neurosci. 2003; 23:4261–4269. [PubMed: 12764114]
84. Biag J, Huang Y, Gou L, Hintiryan H, Askarinam A, Hahn JD, Toga AW, Dong HW. Cyto- and chemoarchitecture of the hypothalamic paraventricular nucleus in the C57BL/6J male mouse: a study of immunostaining and multiple fluorescent tract tracing. J Comp Neurol. 2012; 520:6–33. [PubMed: 21674499]
85. Fernandez-Monreal M, Brown TC, Royo M, Esteban JA. The balance between receptor recycling and trafficking toward lysosomes determines synaptic strength during long-term depression. J Neurosci. 2012; 32:13200–13205. [PubMed: 22993436]

86. Pierce JP, Kievits J, Graustein B, Speth RC, Iadecola C, Milner TA. Sex differences in the subcellular distribution of angiotensin type 1 receptors and NADPH oxidase subunits in the dendrites of C1 neurons in the rat rostral ventrolateral medulla. Neuroscience. 2009; 163:329–338. [PubMed: 19501631]

87. Boudin H, Pelaprat D, Rostene W, Pickel VM, Beaudet A. Correlative ultrastructural distribution of neurotensin receptor proteins and binding sites in the rat substantia nigra. J Neurosci. 1998; 18:8473–8484. [PubMed: 9763490]

88. Ladepeche L, Dupuis JP, Groc L. Surface trafficking of NMDA receptors: gathering from a partner to another. Semin Cell Dev Biol. 2014; 27:3–13. [PubMed: 24177014]

89. Mu Y, Otsuka T, Horton AC, Scott DB, Ehlers MD. Activity-dependent mRNA splicing controls ER export and synaptic delivery of NMDA receptors. Neuron. 2003; 40:581–594. [PubMed: 14642281]

90. Norman ED, Thiels E, Barrionuevo G, Klann E. Long-term depression in the hippocampus in vivo is associated with protein phosphatase-dependent alterations in extracellular signal-regulated kinase. J Neurochem. 2000; 74:192–198. [PubMed: 10617120]

91. Roepke TA, Ronnekleiv OK, Kelly MJ. Physiological consequences of membrane-initiated estrogen signaling in the brain. Front Biosci. 2011; 16:1560–1573.

92. Fan X, Jin WY, Wang YT. The NMDA receptor complex: a multifunctional machine at the glutamatergic synapse. Front Cell Neurosci. 2014; 8:160. [PubMed: 24959120]

93. Cyr M, Ghribi O, Thibault C, Morissette M, Landry M, Di Paolo T. Ovarian steroids and selective estrogen receptor modulators activity on rat brain NMDA and AMPA receptors. Brain Res Brain Res Rev. 2001; 37:153–161. [PubMed: 11744083]

94. Sellers K, Raval P, Srivastava DP. Molecular signature of rapid estrogen regulation of synaptic connectivity and cognition. Front Neuroendocrinol. 2015; 36:72–89. [PubMed: 25159586]

95. Tan XJ, Dai YB, Wu WF, Kim HJ, Barros RP, Richardson TI, Yaden BC, Warner M, McKinzie DL, Krishnan V, Gustafsson JA. Reduction of dendritic spines and elevation of GABAergic signaling in the brains of mice treated with an estrogen receptor beta ligand. Proc Natl Acad Sci USA. 2012; 109:1708–1712. [PubMed: 22307635]

96. Spencer-Segal JL, Tsuda MC, Mattei L, Waters EM, Romeo RD, Milner TA, McEwen BS, Ogawa S. Estradiol acts via estrogen receptors alpha and beta on pathways important for synaptic plasticity in the mouse hippocampal formation. Neuroscience. 2012; 202:131–146. [PubMed: 22133892]

97. McEwen, BS., Milner, TA., Waters, EM. Estrogen effects on hippocampal synapses; in Pickel VM, Segal M (eds): The Synapse Structure and Function. New York: Elsevier; 2014.

98. McEwen BS, Akama KT, Spencer-Segal JL, Milner TA, Waters EM. Estrogen effects on the brain: actions beyond the hypothalamus via novel mechanisms. Behav Neurosci. 2012; 126:4–16. [PubMed: 22289042]

99. Waters EM, Yildirim M, Janssen WG, Lou WY, McEwen BS, Morrison JH, Milner TA. Estrogen and aging affect the synaptic distribution of estrogen receptor beta-immunoreactivity in the CA1 region of female rat hippocampus. Brain Res. 2011; 1379:86–97. [PubMed: 20875808]

100. Yildirim M, Janssen WG, Lou WY, Akama KT, McEwen BS, Milner TA, Morrison JH. Effects of estrogen and aging on the synaptic distribution of phosphorylated Akt-immunoreactivity in the CA1 region of the female rat hippocampus. Brain Res. 2011; 1379:98–108. [PubMed: 20709039]

101. Wu WW, Adelman JP, Maylie J. Ovarian hormone deficiency reduces intrinsic excitability and abolishes acute estrogen sensitivity in hippocampal CA1 pyramidal neurons. J Neurosci. 2011; 31:2638–2648. [PubMed: 21325532]

102. Hanley JG. AMPA receptor trafficking pathways and links to dendritic spine morphogenesis. Cell Adh Migr. 2008; 2:276–282. [PubMed: 19262155]

103. Campos C, Sartorio CL, Casali KR, Fernandes RO, Llesuy S, da Rosa Araujo AS, Bello-Klein A, Rigatto KV. Low-dose estrogen is as effective as high-dose treatment in rats with postmenopausal hypertension. J Cardiovasc Pharmacol. 2014; 63:144–151. [PubMed: 24157955]

104. Van Kempen TA, Narayan A, Waters EM, Marques-Lopes J, Iadecola C, Glass MJ, Pickel VM, Milner TA. Alterations in the subcellular distribution of NADPH oxidase p47 in hypothalamic

paraventricular neurons following slow pressor angiotensin II hypertension in female mice with accelerated ovarian failure. J Comp Neurol. Epub ahead of print.

105. Brandes RP, Weissmann N, Schroder K. Nox family NADPH oxidases: molecular mechanisms of activation. Free Radic Biol Med. 2014; 76:208–226. [PubMed: 25157786]
106. Van Kempen, T., Marques-Lopes, J., Glass, MJ., Milner, TA. Sex differences in neural regulation of hypertension. In: Girouard, H., editor. Hypertension and the Brain as an End-Organ Target. New York: Springer; 2016. p. 195-221.
107. Cardinale JP, Sriramula S, Mariappan N, Agarwal D, Francis J. Angiotensin II-induced hypertension is modulated by nuclear factor-kappaB in the paraventricular nucleus. Hypertension. 2012; 59:113–121. [PubMed: 22106405]
108. Choe KY, Han SY, Gaub P, Shell B, Voisin DL, Knapp BA, Barker PA, Brown CH, Cunningham JT, Bourque CW. High salt intake increases blood pressure via BDNF-mediated downregulation of KCC2 and impaired baroreflex inhibition of vasopressin neurons. Neuron. 2015; 85:549–560. [PubMed: 25619659]
109. Hodis HN, Mack WJ. A ‘window of opportunity’: the reduction of coronary heart disease and total mortality with menopausal therapies is age- and time-dependent. Brain Res. 2011; 1379:244–252. [PubMed: 20977895]
110. Pinkerton JV, Stovall DW. Reproductive aging, menopause, and health outcomes. Ann NY Acad Sci. 2010; 1204:169–178. [PubMed: 20738288]

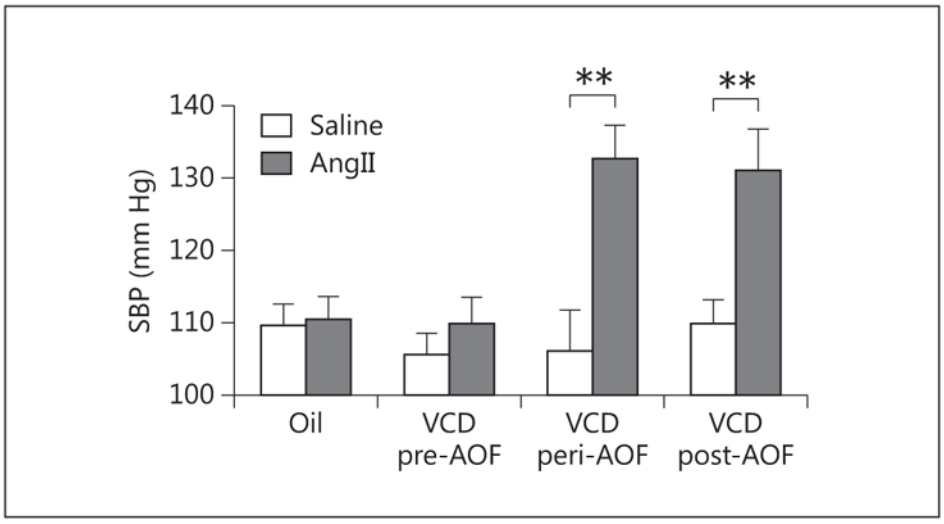


**Fig. 1.**

Slow-pressor AngII increases blood pressure in peri- and post-AOF mice. Thirteen days after minipump implantation, An-gII infusion did not significantly increase ($p > 0.05$) SBP in VCD-injected mice at the pre-AOF time point. However, AngII infusion significantly elevated (** $p < 0.01$) SBP in VCD-injected mice at peri- and post-AOF time points compared to their respective age-matched oil-injected controls. No significant differences in SBP were found in oil/saline (controls) from the pre-, peri- or post-AOF time points. Thus, oil-injected mice are pooled for all AOF time points; n = 4–12 mice/group.

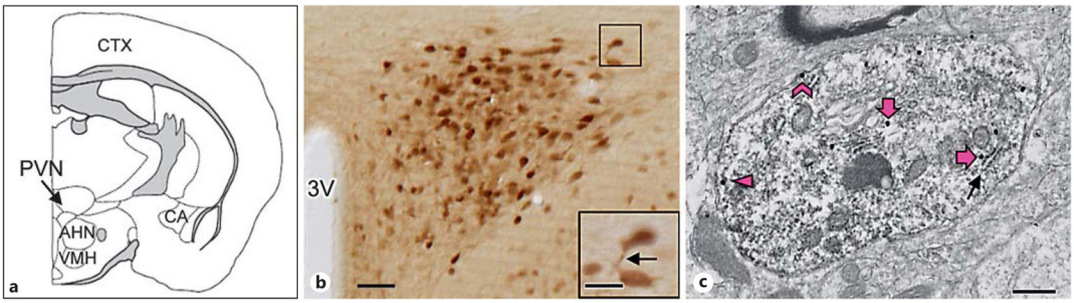


**Fig. 2.**

ERβ-EGFP is expressed in somata and dendrites of PVN neurons including those also containing GluN1. **a** The diagram of a coronal section of the mouse forebrain shows a representative rostrocaudal section at the level of the PVN (modified from Siegel et al. [58] ). CTX = Cerebral cortex; AHN = anterior hypothalamic nucleus; VMH = ventromedial hypothalamus; CA = cornu ammonis. **b** A light-microscopic image of the PVN shows ERβ-EGFP immunoperoxidase labeling in many neuronal somata and putative dendritic processes (example indicated by an arrow in the higher magnification inset). 3V = Third ventricle. Bar = 0.5 mm; inset bar = 25 μm. **c** A representative electron micrograph shows GluN1-SIG particles in an ERβ-EGFP immunoperoxidase-labeled PVN dendrite. A diffuse immunoperoxidase reaction product for ERβ-EGFP is seen as an electron-dense precipitate throughout the cytoplasm of the dendritic profile. GluN1-SIG particles (black dots) are in contact with the plasma membrane (chevron), near (within 70 nm), but not touching the surface membrane (arrowhead) and in the more central cytoplasm (thick arrows). Cytoplasmic GluN1-SIG particles were often adjacent to endomembranes (arrow). Bar = 500 nm.

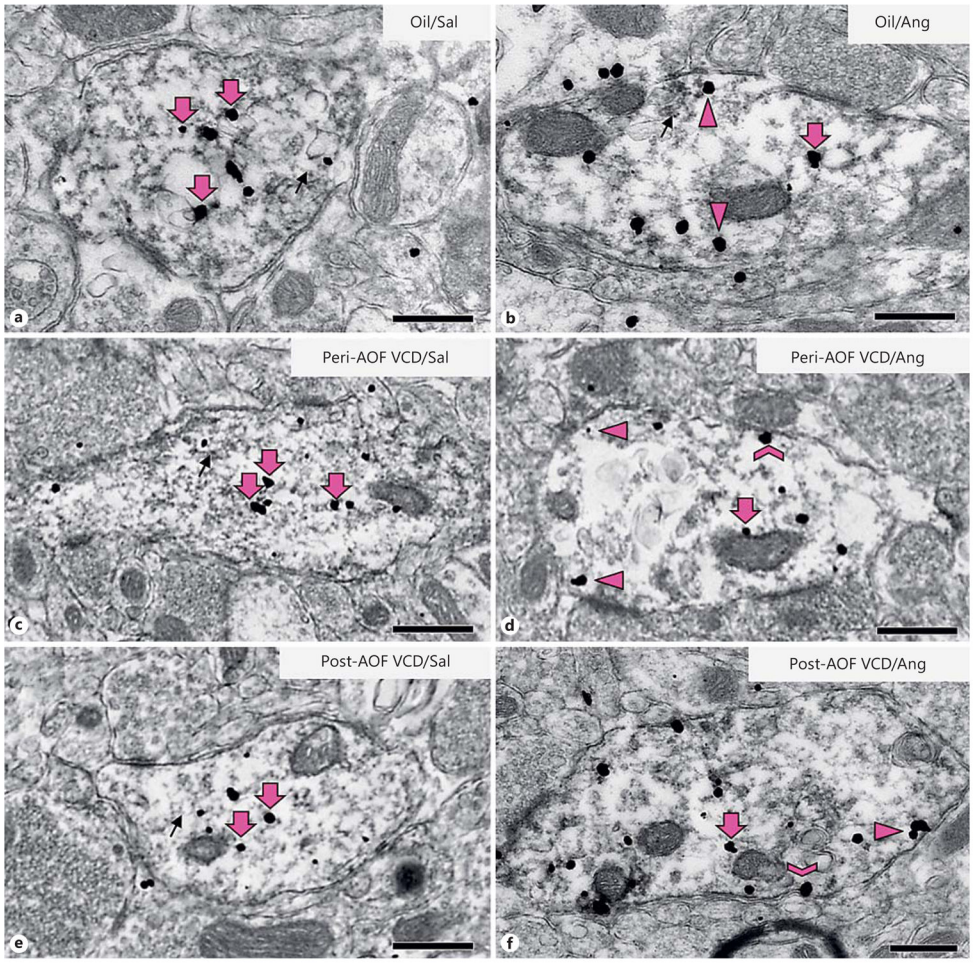


**Fig. 3.**

Representative micrographs of GluN1-SIG localization in ERβ-EGFP dendrites of peri- and post-AOF mice following slow-pressor AngII infusion. Representative electron micrographs of dual-labeled GluN1/ERβ-EGFP dendrites from oil-injected, saline-infused (**a**), oil-injected, AngII-infused (**b**), VCD, saline-infused peri-AOF (**c**), VCD, AngII-infused peri-AOF (**d**), VCD, saline-infused post-AOF (**e** ), and VCD, AngII-infused post-AOF (**f**) female mice. Examples of plasmalemmal (chevron), near-plasma-lemmal (arrowhead) and cytoplasmic (large arrow) GluN1-SIG particles are shown. GluN1-SIG particles were sometimes adjacent to membranous structures (small arrow), especially in oil-injected mice (**a**, **b** ) and in saline-injected peri- and post-AOF VCD mice (**c**, **e**). Bars = 500 nm.

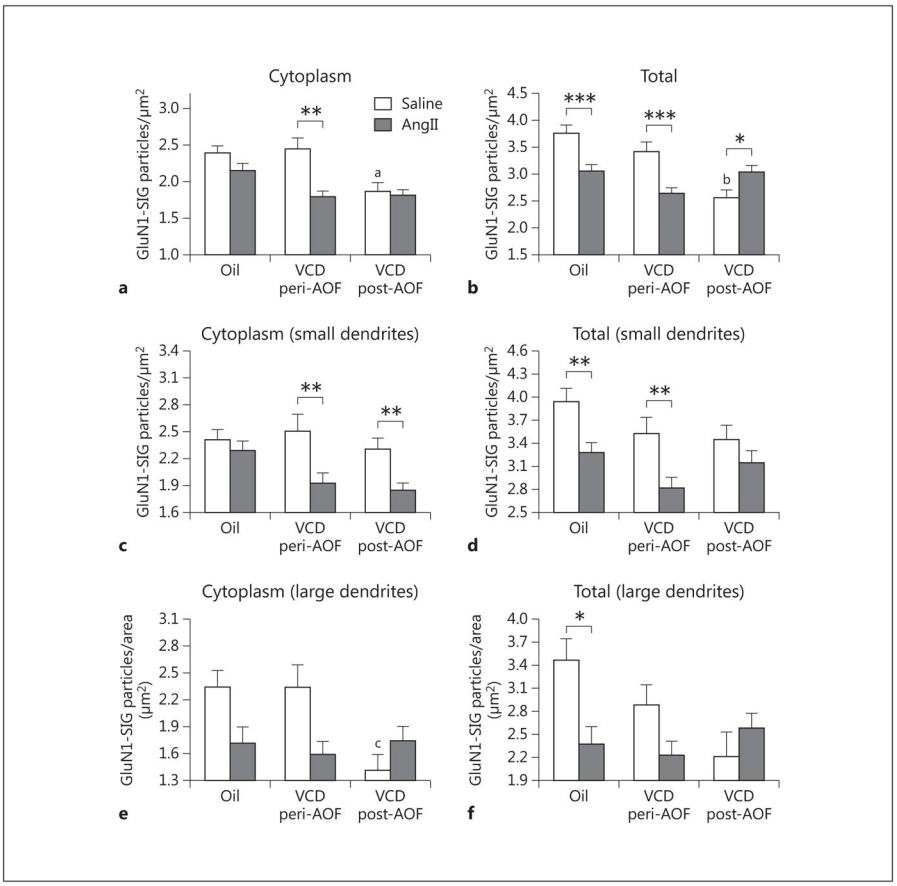


**Fig. 4.**

Slow-pressor AngII infusion differentially affects GluN1 density in ERβ-EGFP dendrites depending on AOF time point. **a** There is a significant decrease in the cytoplasmic density of GluN1-SIG particles in peri-AOF VCD mice following AngII infusion compared to peri-AOF VCD mice receiving saline. **b** The density of total GluN1-SIG particles in peri-AOF VCD mice given AngII compared to their peri-AOF VCD controls receiving saline is significantly reduced. In contrast, the density of total GluN1 particles in post-AOF VCD mice given AngII compared to their post-AOF VCD controls receiving saline is significantly increased. Oil-injected mice receiving AngII show a decrease in total GluN1 compared to those receiving oil and saline. **c** In small (<0.1 μm in diameter) ERβ-EGFP dendrites, AngII infusion results in a decrease in the cytoplasmic density of GluN1-SIG particles in peri- and post-AOF VCD mice. **d** In small ERβ-EGFP dendrites, the total number of GluN1-SIG particles is less in peri- and post-AOF VCD mice compared to oil-injected mice. Following AngII infusion, the density of the total number of GluN1-SIG particles decreases in oil-injected and peri-AOF VCD mice. **e** In large (>0.1 μm in diameter) ERβ-EGFP dendrites, the total number of GluN1-SIG particles in the cytoplasm of ERβ-EGFP dendrites in post-AOF VCD mice is significantly less compared to oil-injected and peri-AOF VCD mice. **f** Following AngII, the total number of GluN1-SIG particles in ERβ-EGFP dendrites significantly decreases in oil-injected mice. * $p < 0.05$; ** $p < 0.01$; ***$p < 0.001$; $^{a}p < 0.05$ compared to saline + oil and saline + VCD peri-AOF; $^{b}p = 0.001$ compared to saline + oil

and $p < 0.01$ compared to saline peri-AOF VCD; [c]$p = 0.01$ compared to saline + oil and saline peri-AOF VCD.

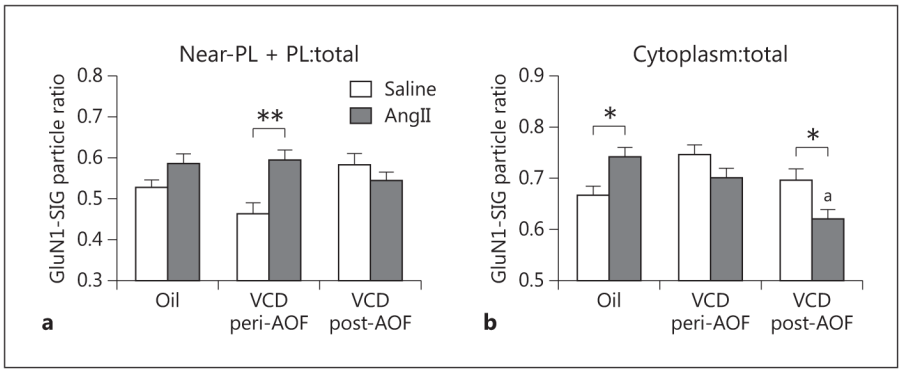


**Fig. 5.**

The AOF time point is a determinant of the differential effects of AngII infusion on the partitioning ratio of GluN1 in plasmalemmal (PL) and cytoplasmic compartments of ERβ-EGFP-containing dendrites. **a** Following AngII infusion, peri-AOF VCD mice have a greater proportion of GluN1-SIG particles in the plasmalemmal + near-plasmalemmal compartments of these dendrites. **b** Following AngII infusion, post-AOF VCD mice have a lower ratio of GluN1-SIG particles in the cytoplasm of ERβ-EGFP dendrites compared to their matched control. Oil-injected mice given AngII have a greater ratio of GluN1-SIG particles in the cytoplasm of ERβ-EGFP dendrites compared to mice receiving oil and saline. *$p < 0.05$; **$p < 0.01$; $^{a}p < 0.001$, post-AOF VCD compared to oil.

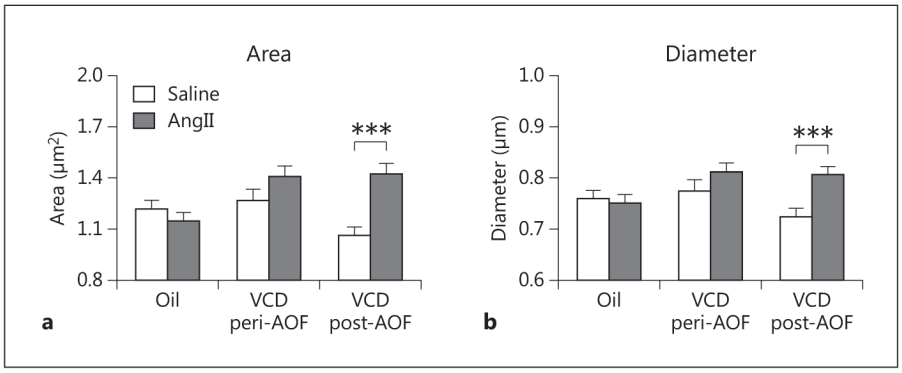


**Fig. 6.**

AngII infusion alters the size of ERβ-EGFP dendrites depending on AOF time point. **a** AngII infusion increases the area of ERβ-EGFP dendrites in post-AOF VCD mice. **b** AngII infusion increases the minimum diameter of ERβ-EGFP dendrites in post-AOF VCD mice. ***$p < 0.001$, post-AOF VCD compared to oil.

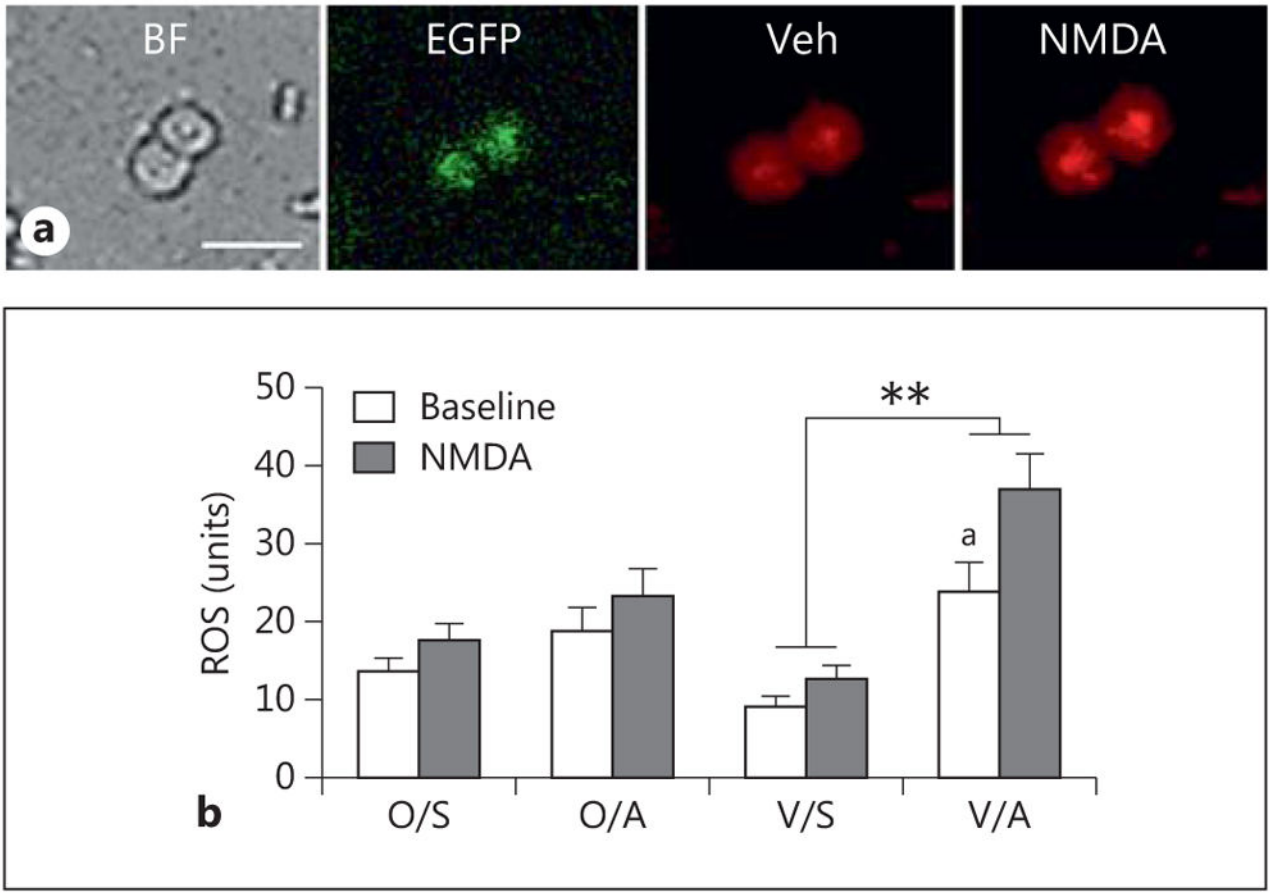


**Fig. 7.**

AngII increases ROS production in isolated ERβ-EGFP-containing PVN neurons in post-AOF mice. **a** Representative images of ERβ-EGFP PVN neurons from an AngII-infused post-AOF female mouse: bright field (BF), EGFP (green) and ROS-dependent fluorescence (red) before (Veh = vehicle) and after the application of NMDA. **b** At baseline, ROS production was significantly greater in AngII-infused VCD mice compared to saline-infused VCD mice ($^{a}p = 0.039$). Application of NMDA (100 μM) significantly elevated ROS production in AngII-infused VCD mice compared to the saline-infused AngII mice (**$p < 0.001$); n = 4–6 mice/group. O = Oil; S = saline; A = AngII; V = VCD.

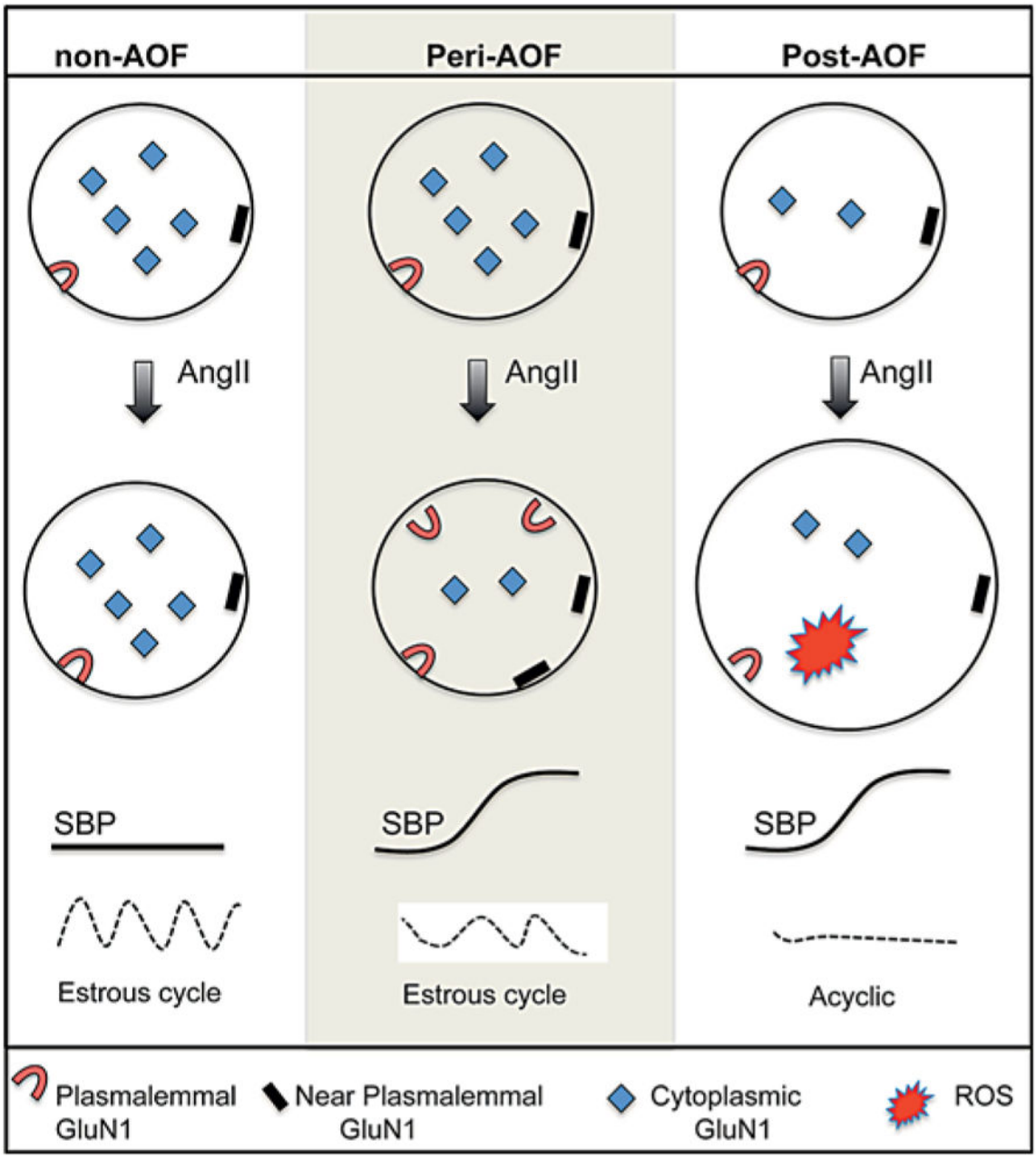


**Fig. 8.**

Schematic diagram summarizing AngII-induced effects on the subcellular distribution of GluN1 in ERβ-EGFP dendrites in the PVN. Slow-pressor AngII elevates SBP in peri- and post-AOF females but not control (oil-injected) females. At the pre-AOF time point, mice have regular estrous cycles. At the peri-AOF time point, estrous cycles are irregular, and at the post-AOF time point, the mice are acyclic. Baseline: oil recipient (non-AOF) and peri-AOF VCD females have a greater density of cytoplasmic GluN1-SIG particles in ERβ-EGFP dendrites (circles) of the PVN than VCD females at the post-AOF time point. Slow-pressor AngII: in oil recipient (nonhypertensive) females, infusion of AngII does not alter the distribution of GluN1-SIG particles in ERβ-EGFP dendrites. In contrast, AngII infusion

in peri-AOF VCD mice reap-portions the GluN1-SIG particles from the cytoplasm to the plasma membrane and near the plasma membrane of ERβ-EGFP dendrites concomitantly with the induction of hypertension. In the post-AOF VCD females, slow-pressor AngII does not redistribute GluN1-SIG particles in ERβ-EGFP dendrites but does increase the size of ERβ-EGFP dendrites and ROS production in ERβ-EGFP neurons.